AD-A085 764 ILLINOIS UNIV AT URBANA-CHAMPAIGN COORDINATED SCIENCE LAB F/G 20/1
SCATTERING MATRIX ANALYSIS OF SURFACE ACOUSTIC WAVE REFLECTORS --ETC(U)
FEB 80 C M PANASIK F19628-78-C-0040
UNCLASSIFIED R-873 NL

END
DATE FILMED
7-80
DTIC

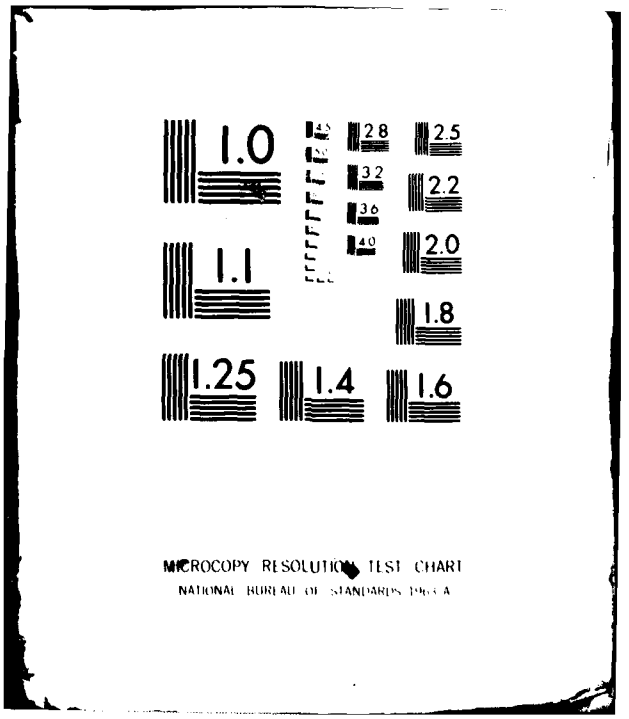
1.0
1.1
1.25
1.4
1.6
1.8
2.0
2.2
2.5
2.8
3.2
3.6
4.0
MICROCOPY RESOLUTION TEST CHART
NATIONAL BUREAU OF STANDARDS 1963-A

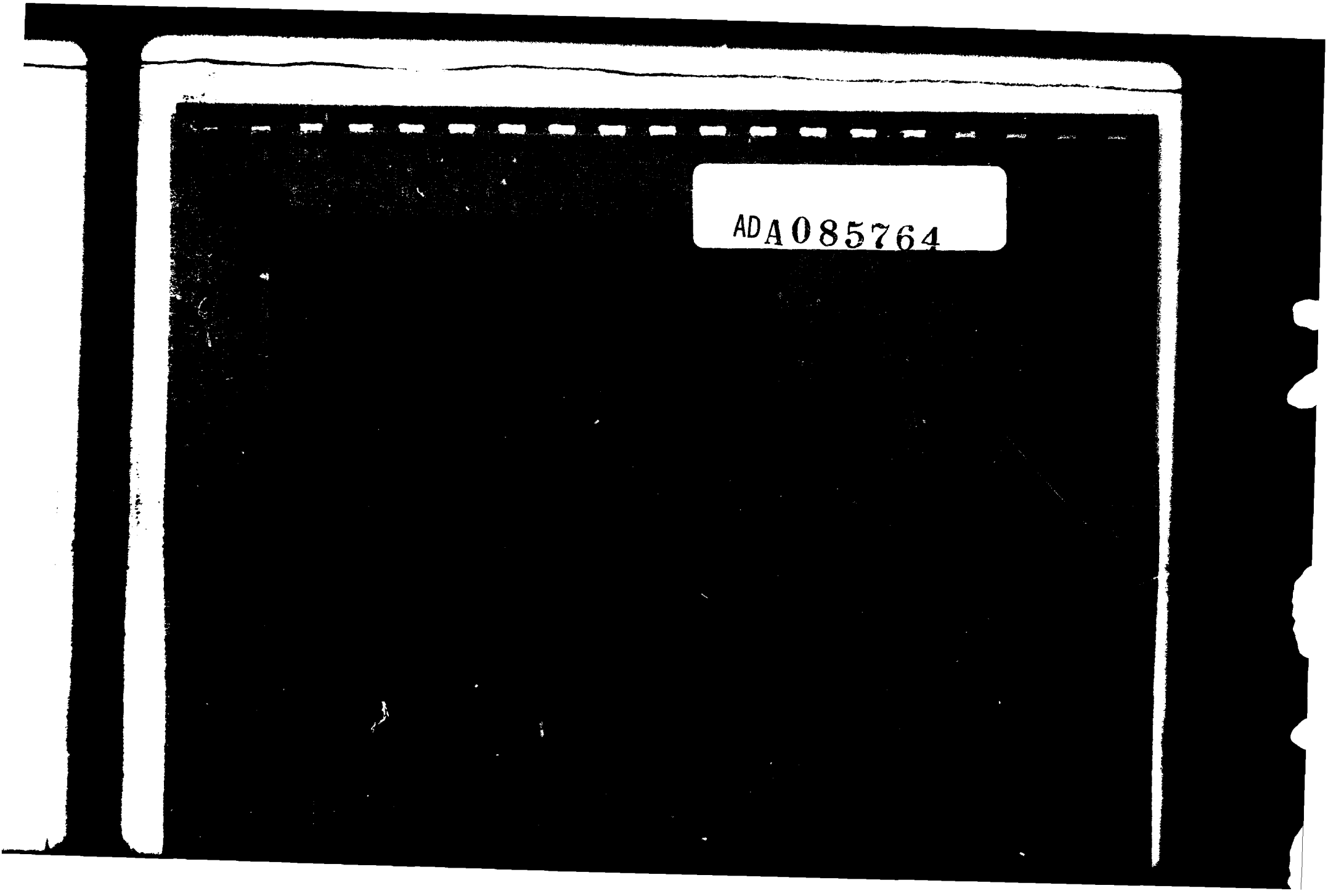

UNCLASSIFIED

SECURITY CLASSIFICATION OF THIS PAGE (When Data Entered)

REPORT DOCUMENTATION PAGE	READ INSTRUCTIONS BEFORE COMPLETING FORM
1. REPORT NUMBER	2. GOVT ACCESSION NO. AD-A085 764	3. RECIPIENT'S CATALOG NUMBER
4. TITLE (and Subtitle) (6) SCATTERING MATRIX ANALYSIS OF SURFACE ACOUSTIC WAVE REFLECTORS AND TRANSDUCERS	5. TYPE OF REPORT & PERIOD COVERED Technical Report
	6. PERFORMING ORG. REPORT NUMBER R-873; UILU-ENG 80-2205
7. AUTHOR(s) (10) Carl Michael Panasik	8. CONTRACT OR GRANT NUMBER(s) (15) F19628-78-C-0040; N00014-79-C-0424
9. PERFORMING ORGANIZATION NAME AND ADDRESS Coordinated Science Laboratory University of Illinois at Urbana-Champaign Urbana, Illinois 61801	10. PROGRAM ELEMENT, PROJECT, TASK AREA & WORK UNIT NUMBERS (12) 701
11. CONTROLLING OFFICE NAME AND ADDRESS Joint Services Electronics Program (11)	12. REPORT DATE Feb 80
	13. NUMBER OF PAGES 61
14. MONITORING AGENCY NAME & ADDRESS (if different from Controlling Office) (14) R-873; UILU-ENG-80-2205	15. SECURITY CLASS. (of this report) UNCLASSIFIED
	15a. DECLASSIFICATION/DOWNGRADING SCHEDULE

16. DISTRIBUTION STATEMENT (of this Report)

Approved for public release; distribution unlimited

(7) Doctoral thesis

17. DISTRIBUTION STATEMENT (of the abstract entered in Block 20, if different from Report)

18. SUPPLEMENTARY NOTES

19. KEY WORDS (Continue on reverse side if necessary and identify by block number)

Surface Acoustic Waves
Filters
Reflectors

20. ABSTRACT (Continue on reverse side if necessary and identify by block number)

The phased periodic array scattering parameters have been modified and corrected for use as a single electrode, mixed units, scattering matrix consisting of one electrical and two acoustic port. These scattering parameter analytical expressions are functions of material constants, electrode geometry, and frequency. The three port single electrode scattering matrices are acoustically cascaded to produce a three port device scattering matrix which takes into account all finger interactions (acoustic and electric) for

DD FORM 1 JAN 73 1473 EDITION OF 1 NOV 65 IS OBSOLETE

UNCLASSIFIED 097100

SECURITY CLASSIFICATION OF THIS PAGE (When Data Entered)

20. (Abstract continued)

the combined effects of piezoelectric and mechanical scattering. The analysis agrees well with experimental measurements of input admittance, electro-acoustic transfer function, and acoustic transmission and reflection coefficients as functions of frequency. Analysis results for the complete modeling of transducers with floating electrodes are also presented.

SCATTERING MATRIX ANALYSIS OF SURFACE ACOUSTIC WAVE REFLECTORS AND TRANSDUCERS

by

Carl Michael Panasik

This work was supported in part by the Joint Services Electronics Program (U.S. Army, U.S. Navy and U.S. Air Force) under Contract N00014-79-C-0424 and the U.S. Air Force under Contract F19628-78-C-0040.

SCATTERING MATRIX ANALYSIS OF SURFACE ACOUSTIC WAVE REFLECTORS AND TRANSDUCERS

BY

CARL MICHAEL PANASIK

B.E.E., The Cleveland State University, 1974
M.S., University of Illinois, 1977

THESIS

Submitted in partial fulfillment of the requirements
for the degree of Doctor of Philosophy in Electrical Engineering
in the Graduate College of the
University of Illinois at Urbana-Champaign, 1980

Thesis Advisor: Professor Bill J. Hunsinger

Urbana, Illinois

SCATTERING MATRIX ANALYSIS OF SURFACE ACOUSTIC WAVE REFLECTORS AND TRANSDUCERS

Carl Michael Panasik, Ph.D.

Coordinated Science Laboratory and

Department of Electrical Engineering

University of Illinois at Urbana-Champaign, 1980

The phased periodic array scattering parameters [1] have been modified and corrected for use as a single electrode, mixed units, scattering matrix consisting of one electrical and two acoustic ports. These scattering parameter analytical expressions are functions of material constants, electrode geometry, and frequency. The three port single electrode scattering matrices are acoustically cascaded to produce a three port device scattering matrix which takes into account all finger interactions (acoustic and electric) for the combined effects of piezoelectric and mechanical scattering. The analysis agrees well with experimental measurements of input admittance, electro-acoustic transfer function, and acoustic transmission and reflection coefficients as functions of frequency. Analysis results for the complete modeling of transducers with floating electrodes are also presented.

ACKNOWLEDGMENT

I wish to thank Professor B. J. Hunsinger for his constant guidance and encouragement throughout the preparation of this thesis. The personal interest in this research shown by Dr. Hunsinger is also appreciated.

I am also indebted to Anthony Lentine for his technical advice and assistance, and to Laura Ruggieri for her assistance.

In particular, I give special thanks to my wife, Bev, for her patience and support throughout these five years of graduate school. Above all, I am thankful for my Lord and Saviour, Jesus Christ. For without His grace this work would not be possible.

TABLE OF CONTENTS

I. Introduction

The modeling of surface acoustic wave transducers and reflectors has been discussed by several authors. Each model is restricted to transducers or reflectors and most are valid over a limited frequency range. This work provides energy conservation based corrections for a mixed units scattering matrix [1,2] recently derived from an infinite array analysis. This thesis is the first publication to present results involving transducers with floating electrodes and is a general analysis which models any periodic device over all frequencies of interest.

This thesis presents a universal analysis of surface acoustic wave transducers and finite length reflectors. The final result of this one dimensional analysis is a 3 x 3 mixed units scattering matrix description of a reflector or transducer whose parameters are functions of frequency.

This analysis:

* is applicable to all periodic structures, where metallization ratio and/or electrode spacing may vary slowly in the direction of propagation;

* models interdigital transducers, regardless of connection circuitry, including arbitrary voltage electrodes, floating electrodes, and electrically loaded reflector arrays;

* is valid for all frequencies of interest;

* is based on analytical expressions involving material constants, electrode geometry and individual electrode circuitry;

* provides the input admittance, electrical to acoustic transfer function and acoustic to acoustic transfer function (transmission and reflection);

* is in a form that directly accepts a recently derived set of mechanical scattering coefficients [27,28].

A number of useful techniques have been developed to analyze SAW reflectors and transducers. A brief summary of these techniques and their features adds insight to the capabilities of this mixed units scattering matrix approach.

Realizing that the location of interdigital electrodes corresponds to the time delayed signal generated by an incident acoustic impulse, several authors have described an impulse response model [3,8,29]. This model is particularly applicable to weak coupling piezoelectric materials where tap to tap interactions are neglected. The electro-acoustic transfer function of each tap is assumed to be flat over the bandwidth of interest and the tap weights are the Fourier transform of a desired frequency response, making first order modeling a simple process. Hartmann extended this model to include the calculation of transducer impedances and the effect of electrical loading on filter response (second order regenerated reflections) via an electrical port equivalent circuit [4,6]. He points out that another frequency dependent acoustic source could be Engan's Fourier series solution [7] for the electrostatic field produced by the electrodes of an infinite array, but limited his analysis to the fundamental response. Arrays which use overlap weighting with a fixed voltage are modeled using a channelized approach similar to one described by Tancrell and Holland [8].

In their initial strong coupling, transmission line analysis Smith et al. [4] presented two infinite array models ("in-line" and "crossed field") derived from the Mason bulk wave transducer equivalent circuit [5]. The selection between the two approaches is based either upon the predominance of an electric field normal or parallel to the surface. Smith and Pedler

[9] extended this work by introducing 1) quarter wavelength transmission line sections of different impedances (values are empirically derived) representing the electrodes and gaps to model acoustic reflections, 2) Engan's source field into their crossed field Mason bulk wave model to analyze harmonics, and 3) missing electrodes and end effects cases to handle finite length arrays. Their source function is the derivative of the normal electric field component with respect to the direction of propagation along the surface. This new source field extends the analysis accurately to odd harmonic operation. The field equations were solved for a number of electrode connection sequences, taking into account next nearest neighbors. The results are presented in tabular form and are handy for design of periodic polarity sequence transducers. The authors suggest that the case of floating electrodes with induced charges is handled by numerically resolving the electrostatic boundary value problem.

Although Smith and Pedler's tables are accurate near odd harmonics, Szabo realized the need for inter-harmonic frequency analysis and applied a Fourier transform of the displacement field as the source function in the spectral weighting model [10]. A set of electro-acoustic transfer functions are calculated numerically using field theory for a number of local electrode environments. These frequency domain curves replace the flat passband response of the delta functions used in the impulse response models and serve as the mathematical link between such models and experimental device behavior. The curves are used in a design prescription to calculate the tap weights for a given frequency response. Closed form expressions of these transfer functions for structures other than arrays of single electrodes are difficult to obtain analytically.

The advent of floating electrodes and capacity weighted transducers brought about the need for a new model which does not require numerically recalculating the field solution for each possible electrode voltage configuration. Datta et al. [11] point out that in general, for the impulse response model, the separation of the transducer response into an element factor and an array factor is not possible, since the charge distribution on each electrode is different because of neighboring electrode effects. They calculated an element factor, referred to as the basic charge distribution, defined as the charge induced in a grounded array with one volt applied to the center tap. The basic charge distribution does not change from tap to tap and extends the impulse model to all harmonics, taking next nearest neighbors into account. This approach, based on closed-form field theory solutions, accurately models the electro-acoustic response of arbitrary electrode voltages and apodized transducers. The weak coupling approximation, on which this work is based, does not allow the prediction of acoustic reflections and frequency shift due to the local electrode shorting of the acoustic potential wave on highly piezoelectric substrates.

Aoki and Ingebrigsten [12] recognized the importance of reflections and frequency shift in an infinite array. They derived the equivalent circuit parameters of the "mixed circuit" model (a modification of Smith's "in-line" model) from the closed form field theory dispersion relations near resonance to obtain a non-empirically based transmission line model. Although neighbor coupling effects when arbitrary voltages are applied (as in floating electrodes and capacity weighted transducers) are neglected, this dispersion relation based (strong coupling) model correctly predicts the transducer acoustic reflection coefficient magnitude as a function of

frequency. This analysis agrees well with experiment near the odd stopbands. The cascaded "mixed circuits" do not produce a stopband at the even harmonics as field theory suggests, therefore Aoki and Hattori [13] added a stored energy "shunt-susceptance transmission-line" model for use at the even harmonics and showed good agreement with experiment for special transducer configurations.

A traveling acoustic wave creates a set of phased voltages on an array of electrodes if acoustic reflections are assumed negligible. The phase difference between electrodes is constant for a given frequency. The scattering matrix of a single electrode in this infinite periodic, phased voltage, environment has been calculated from field theory by Datta and Hunsinger [1]. The scattering matrix elements are analytical expressions which are functions of frequency, metallization ratio, and substrate parameters. The analysis works well on reflectors and multistrip couplers (passive), but does not address the case of transducers in which an arbitrary voltage is applied to each electrode, nor to fixed tap weight transducers at non-synchronous frequencies.

These single electrode piezoelectric scattering coefficients for infinite periodic arrays [1] have been modified for modeling finite length periodic transducer and reflector structures. A single electrode is represented as a 3 x 3 mixed units scattering matrix. These matrices are cascaded (via acoustic ports) to form an N+2 by 3 matrix that describes the device. This matrix is then compacted into a 3 x 3 matrix which completely defines the three port transducer or two port finite length reflector without the use of special case look-up tables or curves. The analysis is based on piezoelectric and mechanical parameters, accounting for both

scattering mechanisms in slowly varying, periodic structures with arbitrary voltages.

In section II. the modifications to the single element scattering parameters along with the conditions required for cascading are described, while the cascading procedure is described in section III. The interpretation of the composite scattering matrix is discussed in section IV. along with a detailed comparison of the analysis with experimental results for reflectors and single (solid) and double (split) electrode transducers with varying loads at any frequency. This section includes a comparison of experiment with theory when the added mechanical scattering is taken into account. Transducers with floating electrodes are discussed in section V., with a conclusion in section VI.

II. Single Electrode Mixed Units Scattering Parameters

This section describes how the scattering parameters [m'] for a phased array transducer (Fig. 1a) are applied to determine the mixed units scattering matrix [m] for a single electrode unit cell in a grounded array (Fig. 1b). The mixed units scattering matrix characterizes the three port unit cell. The two acoustic ports are characterized by positive and negative traveling acoustic waves, while the electrical port is defined in terms of the most conveniently measured parameters, voltage and current. The mixed units scattering parameters for the single electrode, unit cell are of the form

$$\begin{bmatrix} B_i \\ A_{i+1} \\ I_i \end{bmatrix} = \begin{bmatrix} m_{11} & m_{12} & m_{13} \\ m_{21} & m_{22} & m_{23} \\ m_{31} & m_{32} & m_{33} \end{bmatrix} \begin{bmatrix} A_i \\ B_{i+1} \\ V_i \end{bmatrix} \tag{1}$$

where A_i is the positive propagating wave (open surface electrical potential) as it enters the i^{th} electrode, B_{i+1} is the negative propagating wave and I_i is the current induced. The unit cell has the properties of being symmetrical and lossless. The parameters $m_{11} = m_{22}$, $m_{12} = m_{21}$, and $m_{13} = m_{23}$ are dimensionless while $m_{31} = m_{32}$ and m_{33} have the units of mhos. Also, m_{13} is related to m_{31} by a constant (derived in Appendix I.B.).

The single electrode scattering matrix is evaluated from the previously derived phased array results by noting that the single tap and phased array transducers are identical when the impressed voltage (V_0) equals zero. This allows the first two columns of the [m] matrix to be set equal to their phased array matrix counterparts (equation (23) in [1]).

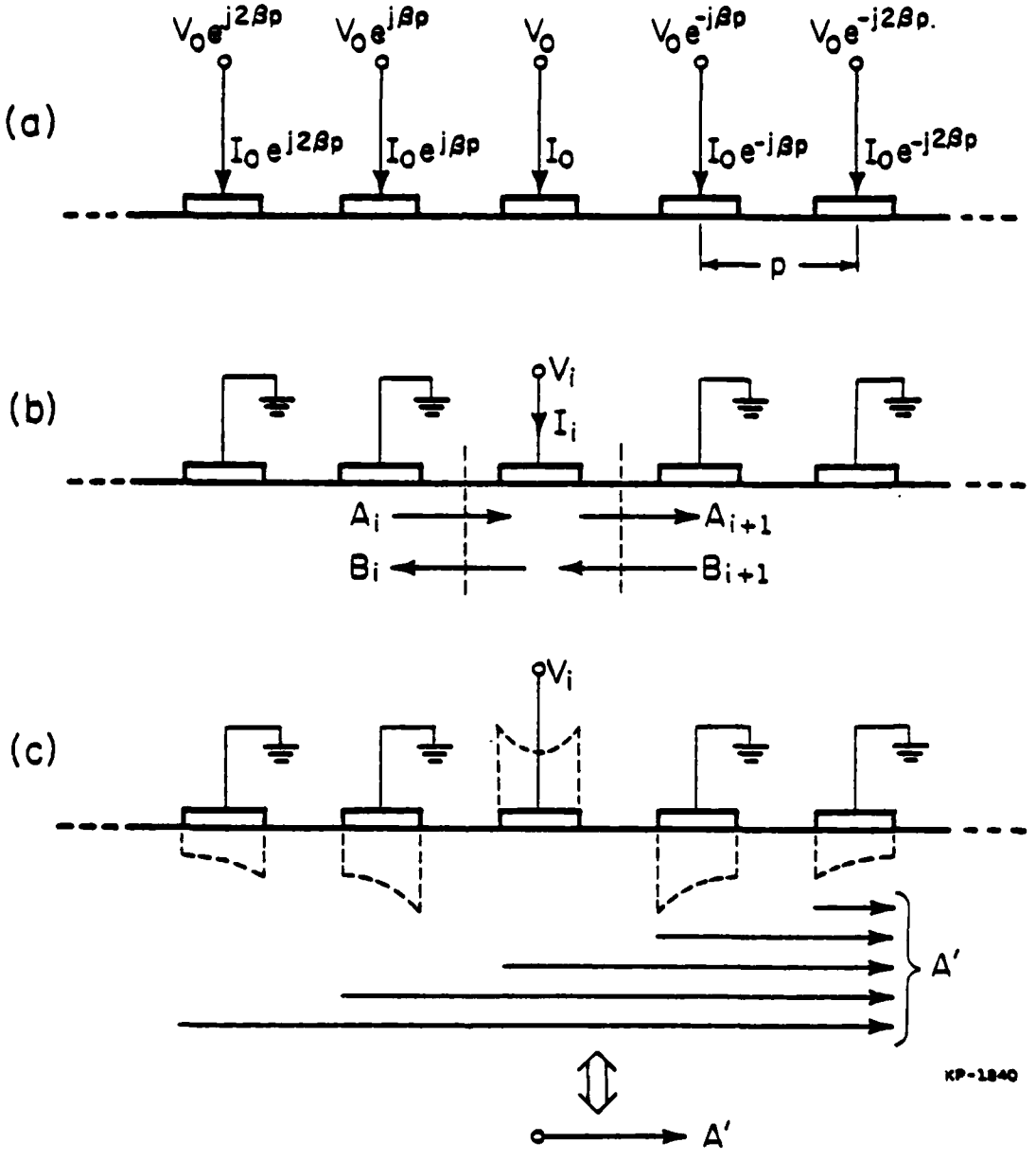

Figure 1. Derivation of single electrode scattering matrix. (a) Phased array transducer. (b) Single electrode in i^{th} position, unit cell. (c) Electro-acoustic transfer mechanism, voltages as in (b) with induced charge (- - -).

When a voltage is applied to one electrode in a grounded array a charge distribution is induced under all adjacent electrodes. Acoustic waves are generated by each of the charged electrodes and the total wave generated is the sum of all the contributions (A') as shown in Fig. 1c. The electro-acoustic transfer function ($m_{13} = m_{23}$) of the i^{th} electrode in a grounded array is defined in terms of the total acoustic wave generated due to the voltage applied. The model assumes that the entire wave is generated in the i^{th} electrode. Each contribution of A' is phase shifted to the center of the i^{th} electrode and summed to give the total electro-acoustic transfer function. The equations for m_{13} and m_{23} are the charge distribution (σ (s,Δ), equation (7) in [2]) multipied by the factor ($\Delta v/v)(p/\epsilon_p+\epsilon_o$) where $\Delta v/v$ is half the piezoelectric coupling coefficient, p is the spacing between electrodes and $\epsilon_p + \epsilon_o$ is the effective substrate dielectric constant.

The current entering the electrode when no incident acoustic waves are present is represented by a complex number (m_{33}, derived in section II.B.). The real part arises due to electrical to acoustic power conversion which is proportional to the coupling coefficient. The imaginary part is the electrostatic capacitive admittance based on the non-piezoelectric properties of the material. For simple periodic voltage transducers (ie. single or double electrode) this capacitance is the capacitance per pair (for example, see equation (14) in [6]), while for devices with arbitrary voltage electrodes, an inter-electrode capacitive admittance matrix (derived from equation (8) and (9) in [2]) is added during the cascading process (section V.).

The weak coupling scattering parameters [m'] (referenced to the electrode center) are tabulated here for convenience.

Acoustic dependent

$$m'_{11} = m'_{22} = j\left|\frac{\Delta v}{v}\right| \cdot 2\pi(s+N).$$

$$\sum_{m=0}^{N} \alpha_m \left[P_{2N+2s-m}(\cos\Delta) + \frac{(-1)^{N-m} P_{N-m+s}(-\cos\Delta)\ P_{N+2s-1}(\cos\Delta)}{P_{s-1}(-\cos\Delta)} \right] \quad (2a)$$

$$m'_{12} = m'_{21} = 1 + j\Delta = 1 + j\left|\frac{\Delta v}{v}\right| \cdot 2\pi(s+N).$$

$$\sum_{m=0}^{N} \alpha_m \left[P_{m-1}(\cos\Delta) + \frac{(-1)^{N-m} P_{N-m+s}(-\cos\Delta)\ P_N(\cos\Delta)}{P_{s-1}(-\cos\Delta)} \right] \quad (2b)$$

$$m'_{31} = m'_{32} = j\omega(\epsilon_p + \epsilon_0) W \cdot 2\pi(s+N).$$

$$\sum_{m=0}^{N} \alpha_m \left[P_{N-m+s}(\cos\Delta) + \frac{(-1)^{N-m} P_{s-1}(\cos\Delta)\ P_{N-m+s}(-\cos\Delta)}{P_{s-1}(-\cos\Delta)} \right] \quad (2c)$$

Voltage dependent

$$m'_{13} = m'_{23} = j\left|\frac{\Delta v}{v}\right| \quad \frac{2\sin\pi s\ P_N(\cos\Delta)}{P_{s-1}(-\cos\Delta)} \quad (2d)$$

where

P_n is the n^{th} Legendre polynomial

$\Delta v/v$ is the half the piezoelectric coupling coefficient

N = integer$(2f/f_o)$

f_o = open surface velocity/electrode spacing = $v/2p$

$s = 2f/f_o - N$

$\Delta = \pi\eta$ (η being the metallisation ratio)

ω is the normalized radian frequency

ϵ_p is the substrate dielectric constant

W is the acoustic beam width

The α_m values are found from equations (9) and (24) in [1]. The derivation of m_{33} is found in section II.B.

This [m'] matrix uses the weak coupling approximation which assumes that the incident (or generated) wave amplitude is constant while traversing the electrode region. This approximation is quite good, however a close inspection of the [m'] matrix will show that energy conservation is not precisely maintained ($|m'_{11}|^2 + |m'_{21}|^2 \neq 1$). Any errors in the original single electrode matrix are accumulated and magnified by the cascading process. Therefore, the initial terms [m'] are corrected (to [m]) by accounting for wave growth under the electrode. A first order effect (2b) is the phase shift ($\delta = j\Delta$) of m'_{21}. As will be shown, the second order correction requires a decrease in the magnitude of m'_{21}. The problem separates into the shorted case (acoustic terms only) and the externally electrical loaded electrode case.

A. Shorted Case

The shorted case involves only the acoustic terms of the mixed unit scattering matrix [m] (essentially an acoustic 2-port), therefore only the upper left corner is addressed

$$\begin{bmatrix} B_1 \\ A_2 \end{bmatrix} = \begin{bmatrix} m_{11} & m_{12} \\ m_{21} & m_{22} \end{bmatrix} \begin{bmatrix} A_1 \\ B_2 \end{bmatrix} \tag{3}$$

The conditions of losslessness for a 2-port require that the net input power to a lossless-passive junction be zero for any combination of excitation possible. That is, there is no energy absorbed in the junction. Therefore, all of the terms of the 2 x 2 scattering hermitian matrix are set to zero (equation (2.22) in [23]). Hence, there are four lossless conditions:

$$\frac{1 - |m_{11}|^2}{Z_{01}} - \frac{|m_{21}|^2}{Z_{02}} = 0 \tag{4a}$$

$$\frac{m^*_{11} m_{12}}{Z_{01}} + \frac{m^*_{21} m_{22}}{Z_{02}} = 0 \tag{4b}$$

$$\frac{1 - |m_{22}|^2}{Z_{01}} - \frac{|m_{12}|^2}{Z_{02}} = 0 \tag{4c}$$

$$\frac{m^*_{12} m_{11}}{Z_{01}} + \frac{m^*_{22} m_{21}}{Z_{02}} = 0 \tag{4d}$$

where Z_{01} and Z_{02} are the transmission line impedances at their respective ports.

These equations with Z_{01} equal to Z_{02} for a symmetrical two port ($m_{11} = m_{22}$ and $m_{12} = m_{21}$) reduce to two equivalent and more revealing forms to be satisfied (equation (2.25) in [23]):

$$1 - |m_{11}|^2 - |m_{21}|^2 = 0 \tag{5a}$$

and

$$\theta_{12} = \theta_{11} + (2n-1)\,\pi/2. \tag{5b}$$

The modification of the acoustic terms involves calculating corrected values of 1) the magnitude of m_{21}, 2) the angle of m_{21} and 3) the angle of m_{11}. The transmission vector of a unit cell without a scattering element (no electrode) is the unit vector t' in Fig. 2. When an electrode is introduced into the unit cell, part of the transmitted wave is continuously scattered as the wave travels under the electrode. The electrode is conceptually divided into many point sources, each being a scatterer of acoustic waves (small arrows in Fig. 2a). The reflections from each section (reverse scattering) experience phase shifts (with refernce to the electrode center) and therefore are summed as phasors (Fig. 2a) to produce m'_{11}. The weak coupling approximation assumes that the transmitted wave traverses each section of the electrode unscattered and accounts for the total forward scattering with the addition of an imaginary scattered wave ($j\Delta$) generated by the electrode (Fig. 2a). This term is negative due to the localized electric field shorting which slows the wave as it propagates under the electrode. When $\delta = j\Delta$ is added to the unit transmission vector, the energy balance (5a) is not satisfied because the magnitude of m'_{21} (=

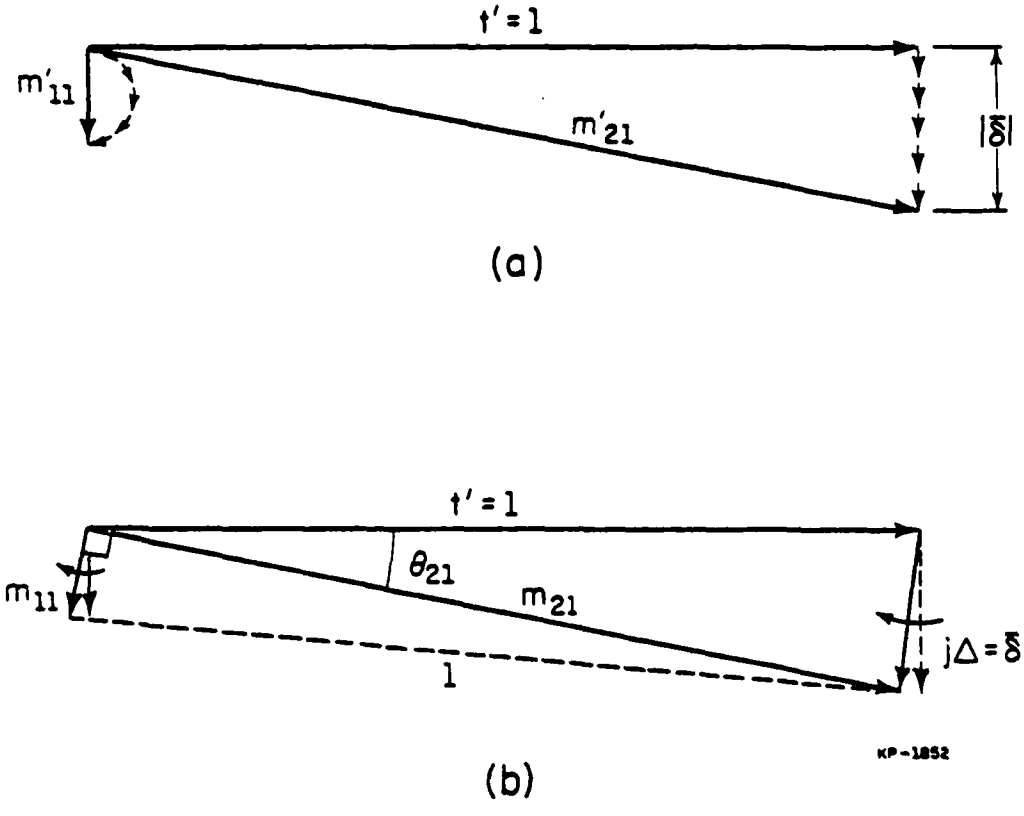

Figure 2. Scattering coefficient vector addition, acoustic terms, shorted case. (a) Weak coupling approximation. (b) Energy conservation correction.

$|1 + j\delta|$) is greater than one. Therefore, δ is rotated (see Fig. 2b) to form one side of a triangle composed of $|\delta|$, the unit vector and the magnitude of m_{21} (as yet unknown).

The first correction is the calculation of the transmitted wave vector (m_{21}) magnitude. This second order correction (decrease in magnitude of m'_{21}) is very small. The magnitude of acoustic reflection (m'_{11}) is also affected by this second order correction (ie. change in all scattering element magnitudes), but since $|m'_{11}| << |m'_{21}|$ the absolute error in $|m'_{11}|$ is near zero (as is the error for all $|m'_{ij}|$, ij $\neq$ 12 or 21). The magnitude of m_{21} is then calculated using (5a) and the magnitude of m'_{11}.

The second step involves calculating the phase angle of the transmitted wave vector angle (θ_{21}) using the unit transmission vector, $|\delta|$ and $|m_{21}|$. The law of cosines is applied to the triangle formed by these three vectors (Fig. 2b)

$$\theta_{21} = \cos^{-1}\left[\frac{|m_{21}|^2 + 1^2 - |\delta|^2}{2 \quad |m_{21}| \quad 1}\right] \tag{6}$$

giving the angle of m_{21} referenced to the electrode center. The transmission phase delay across the unit cell is implemented by adding a $\pi f/f_o$ phase shift, thus giving the corrected angle of m_{21}. Equation (5b) for a symmetrical two port results in $m_{11} \perp m_{21}$ and $m_{22} \perp m_{12}$. Therefore for the third correction (5b), the angle of m_{11} is adjusted to be $\pi/2$ radians from θ_{21}. The two port acoustic scattering matrix now satisfies the lossless conditions.

B. Externally Electrical Loaded Electrode Case

At this point there are 6 corrections remaining: the angles of m_{13}, m_{23}, m_{31}, m_{32} and the complex value of m_{33}. Taking the solution of m_{33} first, from energy considerations it is shown in appendix I.A. that the electrical port radiation conductance is

$$G_a = Re(m_{33}) = -.5(m_{13}m^*_{31} + m_{23}m^*_{32}) \tag{7}$$

If Z_0 is defined as the characteristic electro-acoustic impedance:

$$Z_0 = \frac{|A_1|^2}{2\,P_a} \tag{8}$$

where A_1 is the open surface electric potential and P_a is the total acoustic power flow, then using (appendix I.B.)

$$m_{13} = -\frac{Z_0\, m_{31}}{2} \tag{9}$$

we find that

$$G_a = \frac{2\, m_{13}m^*_{31}}{Z_0} \tag{10}$$

for a symmetrical lossless 3-port and is independent of any scattering coefficient angle. The imaginary part of electrical port input admittance arises from both electrostatic (capacitive) and acoustic generation. The acoustic contribution (B_a) is the Hilbert transform of the real electrical port admittance [30]. For a single electrode the value of B_a is near zero, because the Hilbert transform of a slowly varying G_a is very small. Therefore, the imaginary part of m_{33} is only the admittance due to the capacitance of the unit cell electrode. For a single electrode transducer,

the capacitance of an electrode pair (C_p) is equal to the capacitance of one electrode in an alternately connected array. The total single electrode admittance is then

$$m_{33} = \frac{2\, m_{13} m^*_{31}}{Z_0} + j\omega C_p \tag{11}$$

The solution of the 4 unknown electro-acoustic angles is now addressed. The problem is simplified by the property of a symmetrical 3-port in which

$$m_{31} = m_{32} \tag{12a}$$

and

$$m_{13} = m_{23} \tag{12b}$$

These two equations along with (9) reduce the problem to one unknown angle (for instance, θ_{13}) from which the three other angles are found.

The solution of an equation containing θ_{13} (= $\arg(m_{13})$) involves finding the 2-port matrix equivalent to the 3-port matrix when the third port is electrically terminated in a load (Y_L). Mathematically, the load is absorbed into the third port electrical admittance. Setting the electrical port external current equal to the load current ($-VY_L$) and solving for the normalized voltage at that port induced by an incoming acoustic wave (note $B_2 = 0$) gives:

$$\begin{bmatrix} B_1 \\ A_2 \\ -VY_L \end{bmatrix} = \begin{bmatrix} m_{11} & m_{12} & m_{13} \\ m_{21} & m_{22} & m_{23} \\ m_{31} & m_{32} & m_{33} \end{bmatrix} \cdot \begin{bmatrix} A_1 \\ 0 \\ V \end{bmatrix} \tag{13}$$

The last equation

$$-VY_L = m_{31}A_1 + m_{33}V \tag{14a}$$

after re-arrangement and the use of (8), produces the normalized voltage

$$\frac{V}{A_1} = \frac{-m_{31}}{m_{33}+Y_L} = \frac{-2\,m_{13}}{Z_0(m_{33}+Y_L)} \tag{4b}$$

Inserting this relation into the first row as the generating voltage gives the reflection coefficient ($m_{11\,el}$)

$$\frac{B_1}{A_1} = m_{11} + \frac{m_{13}V}{A_1} = m_{11} - \frac{2\,m_{13}^2}{Z_0\,(m_{33}+Y_L)} = m_{11el} \tag{15a}$$

Similarly, for the transmitted wave

$$\frac{A_2}{A_1} = m_{21} - \frac{2\,m_{13}^2}{Z_0\,(m_{33}+Y_L)} = m_{21el} \tag{15b}$$

Therefore the electrically loaded acoustic scattering matrix (supression of the third port) is represented as

$$\begin{bmatrix} B_1 \\ A_2 \end{bmatrix} = \begin{bmatrix} m_{11el} & m_{12el} \\ m_{21el} & m_{22el} \end{bmatrix} \begin{bmatrix} A_1 \\ B_2 \end{bmatrix} \tag{16}$$

The same symmetrical lossless 2-port equations (5a,b) apply to this matrix. Equation (5a)

$$|m_{11el}|^2 + |m_{21el}|^2 - 1 = 0 \tag{17a}$$

is now

$$\left| m_{11} - \frac{2\,m_{13}^2}{Z_0\,(m_{33}+Y_L)} \right|^2 + \left| m_{21} - \frac{2\,m_{13}^2}{Z_0\,(m_{33}+Y_L)} \right|^2 - 1 = 0 \tag{17b}$$

which simplifies to

$$\mathrm{Re}(m_{11} + m_{21}) \cos \theta_{13} + \mathrm{Im}(m_{11} + m_{21}) \sin \theta_{13} - \frac{|2\, m_{13}{}^2|}{|Z_0\, (m_{33}+Y_L)|} = 0 \tag{17c}$$

giving

$$\theta_{13} = 2\left[\theta_{33} + \theta_{(m_{11}+m_{21})} - \cos^{-1}\left[\frac{|2\, m_{13}{}^2/(Z_0(m_{33}+Y_L))|}{|m_{11} + m_{21}|}\right]\right] \tag{17d}$$

The resulting angle and the use of (9) and (12) give the values of the four unknown angles. As a check, the angle of m_{11el} is compared with the angle of m_{21el} and found to satisfy (5b).

In summary, the corrected mixed units scattering coefficients referenced to the edges of the unit cell (Fig. 1b) are:

$$m_{11} = m_{22} = |m'_{11}|\, e^{j(\theta_{12} \pm \pi/2)}\, e^{-j\pi f/f_o} \tag{18a}$$

$$m_{21} = m_{12} = (\, 1 - |m'_{11}|^2)^{\,1/2}\, e^{j\theta_{12}}\, e^{-j\pi f/f_o} \tag{18b}$$

$$m_{13} = m_{23} = |m'_{13}|\, e^{j\theta_{13}}\, e^{-j\pi f/2f_o} \tag{18c}$$

$$m_{31} = m_{32} = |m'_{31}|\, e^{j(\theta_{13} - \pi)}\, e^{-j\pi f/2f_o} \tag{18d}$$

$$m_{33} = G_a + j\omega\, C_p \tag{18e}$$

These single electrode scattering matrix coefficients conserve energy for acoustic reflection, generation and detection. In the calculation of a finite length device matrix, many single electrode matrices are cascaded and the final device matrix satisfies the three port energy conservation equations (equation (2.165) in [26]).

III. Composite Transducer Matrix

A. Cascading

In order to analyze an entire transducer, the effects of individual fingers and their interactions must be combined, while taking into account the finger connection sequence. This is done by cascading 3-port mixed units, single electrode [m] scattering matrices (18) and then compacting the final matrix into a 3 x 3 matrix [M] describing the total array (Fig. 3).

$$\begin{bmatrix} B_1 \\ A_{N+1} \\ I_T \end{bmatrix} = \begin{bmatrix} M_{11} & M_{12} & M_{13} \\ M_{21} & M_{22} & M_{23} \\ M_{31} & M_{32} & M_{33} \end{bmatrix} \begin{bmatrix} A_1 \\ B_{N+1} \\ V_T \end{bmatrix} \tag{19}$$

The scattering matrix cascading process starts with a single element scattering matrix $[m^1]$ (Fig. 4, equation (20)). This matrix is combined with another adjacent $[m^2]$ matrix which may be different than the first.

$$\begin{bmatrix} B_1 \\ A_2 \\ I_1 \end{bmatrix} = \begin{bmatrix} m^1_{11} & m^1_{12} & m^1_{13} \\ m^1_{21} & m^1_{22} & m^1_{23} \\ m^1_{31} & m^1_{32} & m^1_{33} \end{bmatrix} \begin{bmatrix} A_1 \\ B_2 \\ V_1 \end{bmatrix} \quad \begin{bmatrix} B_2 \\ A_3 \\ I_2 \end{bmatrix} = \begin{bmatrix} m^2_{11} & m^2_{12} & m^2_{13} \\ m^2_{21} & m^2_{22} & m^2_{23} \\ m^2_{31} & m^2_{32} & m^2_{33} \end{bmatrix} \begin{bmatrix} A_2 \\ B_3 \\ V_2 \end{bmatrix} \tag{20}$$

The acoustic interface between the two unit cells contains two unknown interacting acoustic waves A_2 and B_2. The two sets of scattering equations (20) also have two equations relating A_2 and B_2. These 2 equations and 2 unknowns are solved for A_2 and B_2 in terms of A_1, B_3, V_1 and V_2. These are

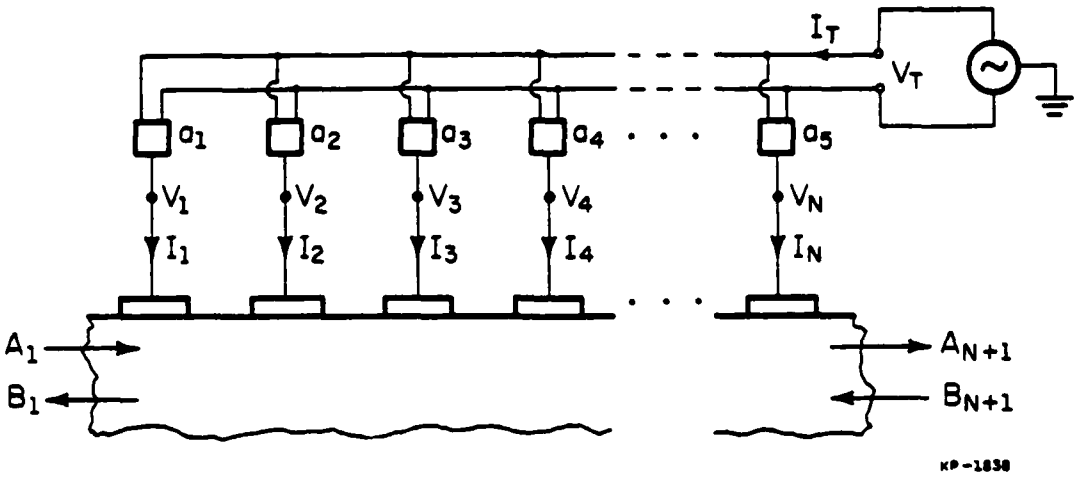

Figure 3. Generalized weighted transducer driven by balanced voltage source.

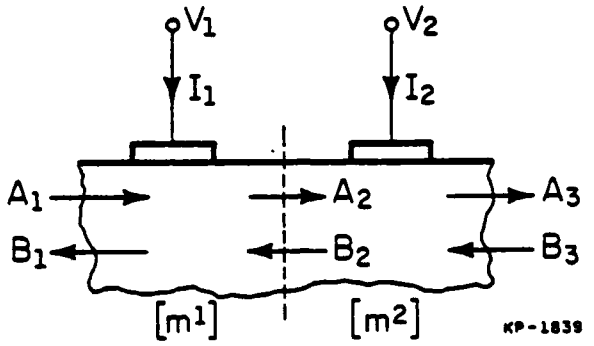

Figure 4. Two electrodes with interacting acoustic potentials.

substituted into their respective locations and a new 4 x 4 scatter matrix is produced which relates the electrode pair input quantities to the output quantities.

$$\begin{bmatrix} B_1 \\ A_3 \\ I_1 \\ I_2 \end{bmatrix} = \begin{bmatrix} m'_{11} & m'_{12} & m'_{13} & m'_{14} \\ m'_{21} & m'_{22} & m'_{23} & m'_{24} \\ m'_{31} & m'_{32} & m'_{33} & m'_{34} \\ m'_{41} & m'_{42} & m'_{43} & m'_{44} \end{bmatrix} \begin{bmatrix} A_1 \\ B_3 \\ V_1 \\ V_2 \end{bmatrix} \tag{21}$$

This new matrix describing the electrode pair now becomes the left matrix and another 3 x 3 matrix representing the third electrode is combined with it. Each matrix has an equation relating the interacting acoustic potentials (now A_3 and B_3) in terms of A_1, B_4, V_1, V_2, and V_3. The 2 equations with 2 unknowns are solved and a new 5 x 5 scattering matrix for the electrode triplet is created. This process continues until the final N+2 by N+2 array scattering matrix is found for an N electrode device (Fig. 3).

$$\begin{bmatrix} B_1 \\ A_{N+1} \\ I_1 \\ I_2 \\ \cdot \\ \cdot \\ \cdot \\ I_N \end{bmatrix} = \left[\begin{array}{cccccc} m_{11} & m_{12} & m_{13} & m_{14} & \cdots \\ m_{21} & m_{22} & m_{23} & m_{24} & \cdots \\ m_{31} & m_{32} & m_{33} & m_{34} & \cdots \\ m_{41} & m_{42} & m_{43} & m_{44} & \cdots \\ \cdot & \cdot & \cdot & \cdot & \cdots \\ \cdot & \cdot & \cdot & \cdot & \cdots \\ \cdot & \cdot & \cdot & \cdot & \cdots \\ \cdot & \cdot & \cdot & \cdot & \cdots \end{array}\right] \begin{bmatrix} A_1 \\ B_{N+1} \\ V_1 \\ V_2 \\ \cdot \\ \cdot \\ \cdot \\ V_N \end{bmatrix} \tag{22}$$

As stated previously, for devices with periodic electrode voltages, the capacitive admittance is included in the single electrode scattering matrix. For devices with arbitrary voltages, a sub matrix of capacitive admittances (D_n from equations (8), (9) in [2]) is added to the admittance sub matrix due to acoustic generation (dashed line in (22)). That is, for i>2 and j>2

$$m_{ij\ \text{total}} = m_{ij\ \text{acoustic}} + D_{|i-j|} \tag{23}$$

This matrix (22) completely describes the interactions between the incoming acoustic traveling wave potentials, the voltages impressed on the electrodes and the outgoing acoustic traveling wave potentials and the electric port induced currents. Appendix II. contains a more detailed description of the cascading process.

B. Compacting

The array scattering matrix can describe any periodic surface wave device taking into account the connection sequence. In an interdigital transducer (IDT) the electrode connection sequence (and therefore each tap voltage) is known apriori. Each of the electrode voltages is related to the terminal voltage (V_T) by a voltage tap weight a_i (Fig. 3), where

$$a_i=(V_i/V_T) \tag{24}$$

Therefore in (22), $m_{1,i>2}$ may be replaced by

$$\begin{aligned} m'_{13} &= m_{13}a_1 + m_{14}a_2 + m_{15}a_3 + \cdots \\ m'_{23} &= m_{23}a_1 + m_{24}a_2 + m_{25}a_3 + \cdots \\ &\vdots \end{aligned} \tag{25}$$

and the n>2 columns are compacted into one.

$$\begin{bmatrix} B_1 \\ A_{N+1} \\ I_1 \\ I_2 \\ \vdots \\ I_N \end{bmatrix} = \begin{bmatrix} m_{11} & m_{12} & m'_{13} \\ m_{21} & m_{22} & m'_{23} \\ m_{31} & m_{32} & m'_{33} \\ m_{41} & m_{42} & m'_{43} \\ \vdots & \vdots & \vdots \\ \cdots & \cdots & \cdots \end{bmatrix} \begin{bmatrix} A_1 \\ B_{N+1} \\ V_T \end{bmatrix} \tag{26}$$

Therefore, if the tap voltages are known, the largest matrix is N+2 by 3 (as shown in appendix II.).

This matrix is compacted by row as well. The terminal current (I_T in Fig. 3) is the sum of the currents in the electrodes connected to one bus bar. This current compacting is approached in much the same way as the voltage compacting. Let b_i be the current tap weight, that is the portion of the electrode current generated by the incident acoustic wave that flows into the positive bus bar (ie. high side, I_T in Fig. 3). In most IDT structures (but not capacitive weighted) b_i will be either 0 or 1. In a single electrode IDT every other b_i is 1 because every other electrode is connected to the high side. Therefore, $m_{3,i>2}$ is replaced by

$$\begin{aligned} m''_{31} &= m_{31}b_1 + m_{41}b_2 + m_{51}b_3 + \cdots \\ m''_{32} &= m_{32}b_1 + m_{42}b_2 + m_{52}b_3 + \cdots \\ m''_{33} &= m'_{33}b_1 + m'_{43}b_2 + m'_{53}b_3 + \cdots \end{aligned} \tag{27}$$

and the m>2 rows are compacted into one.

$$\begin{bmatrix} B_1 \\ A_{N+1} \\ I_T \end{bmatrix} = \begin{bmatrix} m_{11} & m_{12} & m'_{13} \\ m_{21} & m_{22} & m'_{23} \\ m''_{31} & m''_{32} & m''_{33} \end{bmatrix} \begin{bmatrix} A_1 \\ B_{N+1} \\ V_T \end{bmatrix} \tag{28}$$

The result is the desired 3 x 3 mixed units scattering matrix (19) which completely describes the transducer as a three port.

IV. Scattering Matrix Analysis of Transducers and Reflectors

The knowledge of the total scattering matrix for a given surface wave device tap configuration is a very powerful analysis tool. A number of examples will be examined to show its usefulness.

A. Transducer Acoustic Reflection Coefficient

The acoustic reflection coefficient of an electrically loaded transducer is derived from the array scatter matrix (19), (28). The shorted transducer ($V_T = 0$) reflection coefficient due to MEL reflections* is M_{11}. The reflection coefficient of an electrode (or transducer) loaded by an admittance is composed of two parts, the MEL reflection and a regenerated wave. This regenerated wave is produced by the induced voltage at the electrical port arising from an incident wave. To calculate this voltage for the case of a transducer, B_{N+1} is set equal to zero, I_T is the load current ($-V_T Y_L$) and V_T is solved for as in the single electrode case (13), (14) and (15). The M matrix equations are written as

$$\begin{aligned} B_1 &= M_{11}A_1 + M_{13}V_T \\ -V_T Y_L &= M_{31}A_1 + (M_{33}+Y_L)V_T \end{aligned} \tag{29}$$

Solving the second equation for the terminal voltage gives

$$V_T = \frac{-M_{31}\, A_1}{M_{33}+Y_L} \tag{30}$$

Inserting this into the first equation results in

$$B_1 = M_{11}\, A_1 - \frac{M_{13}M_{31}}{M_{33}+Y_L}\, A_1 \tag{31a}$$

---

* Reflections from shorted electrodes (Mechanical-Electrical Loading).

and the electrically loaded reflection coefficient is

$$r_{el} = M_{11} - \frac{M_{13}M_{31}}{M_{33}+Y_L} \quad . \tag{31b}$$

As an example, the complex reflectance for a 20-pair, single electrode (Fig. 5, inset), 0.5 duty factor (metallization ratio) uniform weighted transducer on Y-Z lithium niobate [14] is plotted for two loads in Fig. 5. These calculations show a calculated frequency dependent reflection coefficient whose shape has good agreement with experiment. The authors [15] attributed a similar difference in magnitude between theory and experiment to the measurement method. This calculated response also agrees with that calculated by Aoki and Ingebrigsten (Fig. 4 in [12]).

B. Transducer Radiation Conductance

The transducer radiation conductance G_a (the real part of M_{33}) includes the effects of regeneration, stored energy and other tap interactions. The input conductance of a 78-pair, 0.5 duty factor, unweighted linear transducer on Y-Z lithium niobate has been calculated and is compared in Fig. 6 with the experimental results for a 30 MHz device [16]. The theoretical calculation agrees very well with experiment. Previous theories did not predict the velocity change under the electrodes. Although Jones et al. had calculated the magnitude accurately, they were not able to predict the 1.7% frequency shift down from f_o without any post-calculation fitting.

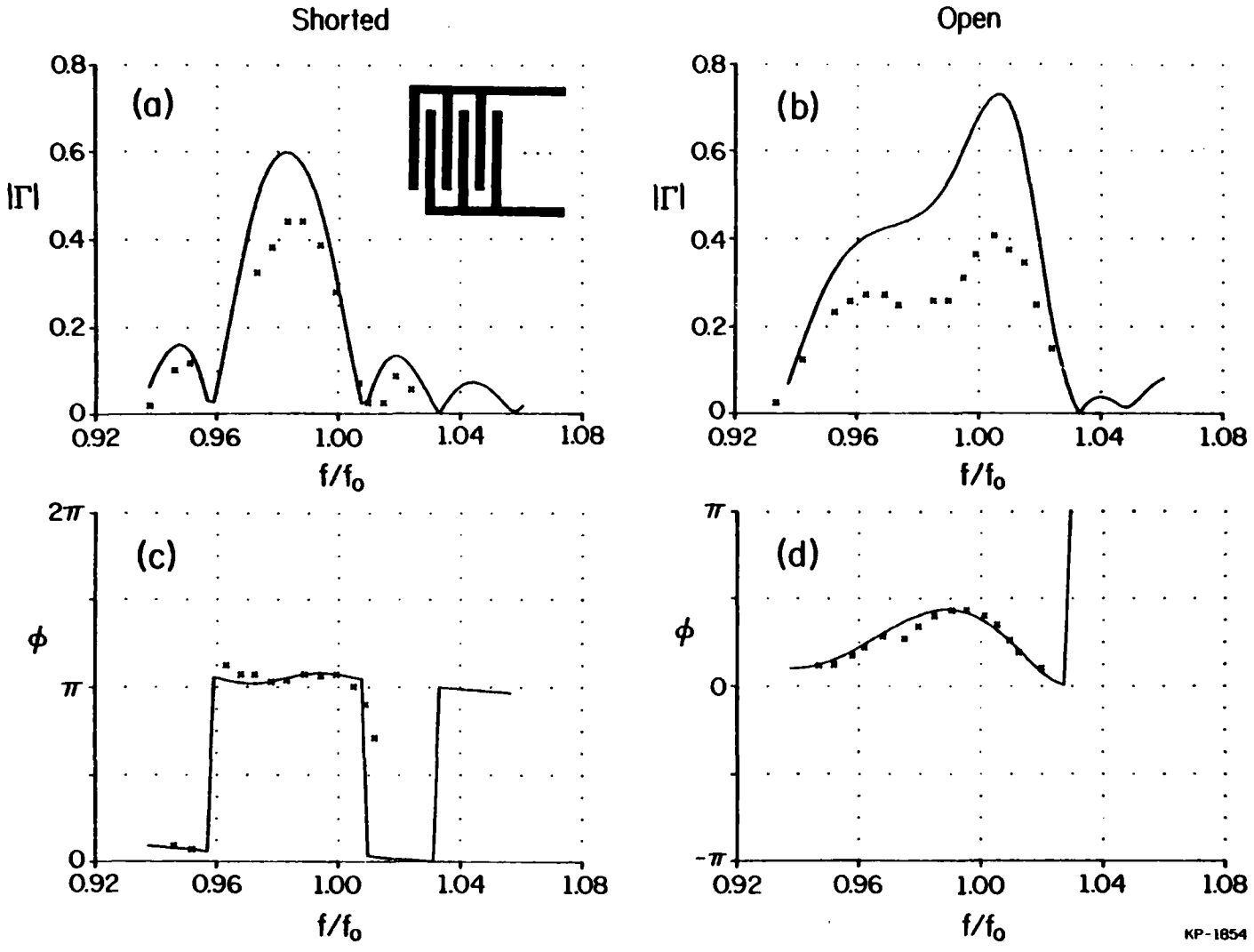

Figure 5. Single electrode transducer, acoustic reflection coefficient. (a) Short circuit magnitude. (b) Open circuit magnitude. (c) Short circuit phase. (d) Open circuit phase.

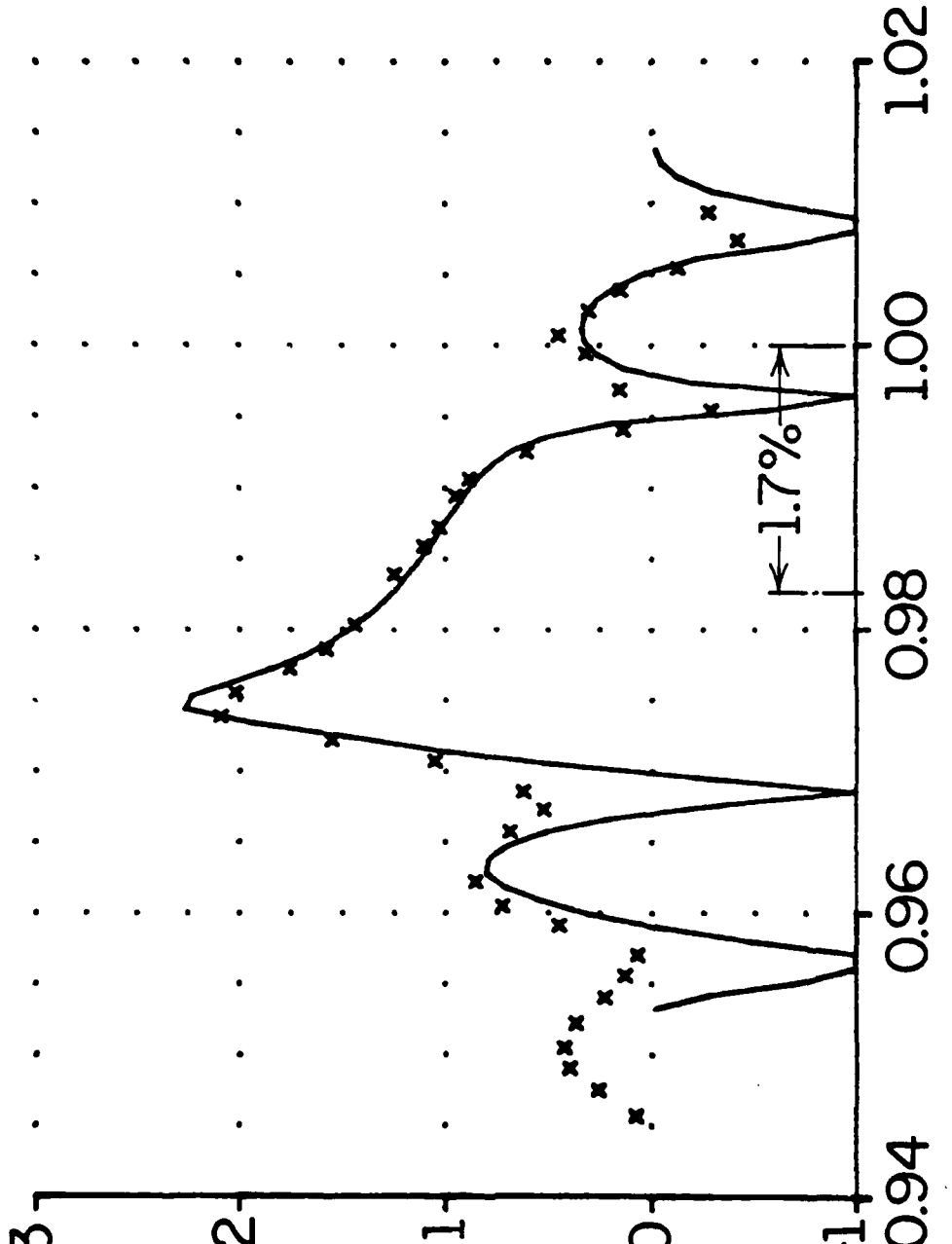

Figure 6. Radiation conductance (Ga) of a 78-pair unwieghted linear transducer.

Calculated radiation conductance for a 15-pair, 0.5 duty factor, double electrode transducer is plotted in Fig. 7 and shows good agreement with experiment [20]. The center frequency of this device is assumed to be 49.44 MHz.

C. Reflector Analysis

The scattering matrix approach lends itself readily to the analysis of reflectors. The acoustic reflection coefficient of a shorted reflector is the same as that of a shorted transducer. The reflection coefficient of an open isolated electrode reflector is unlike that of an open circuited (no load) transducer, although the reflection mechanisms (MEL and regenerated wave) are the same. In the case of isolated electrodes, each electrode operates as an independent (no electrical load) reflector whose induced voltage is a function of the incident acoustic potential. It is convenient here to introduce a neutral reference potential. For an IDT this neutral reference is located half way between electrodes of opposite polarity, so that one half the terminal voltage exists between each terminal and neutral. Admittances are now defined from each electrode to the neutral reference. At fundamental the capacitance of each electrode to the neutral reference is twice the electrode to electrode capacitance used previously.

$$m_{33\ iso} = G_a + 2j\omega C_p \tag{32}$$

The single electrode three port is reduced to a two port by supressing the electrical port. The electrically loaded equations (14-16) ($Y_L = 0$) are evaluated with the isolated admittance (32) and replace the shorted acoustic terms (3) in the single electrode scattering matrix [m]

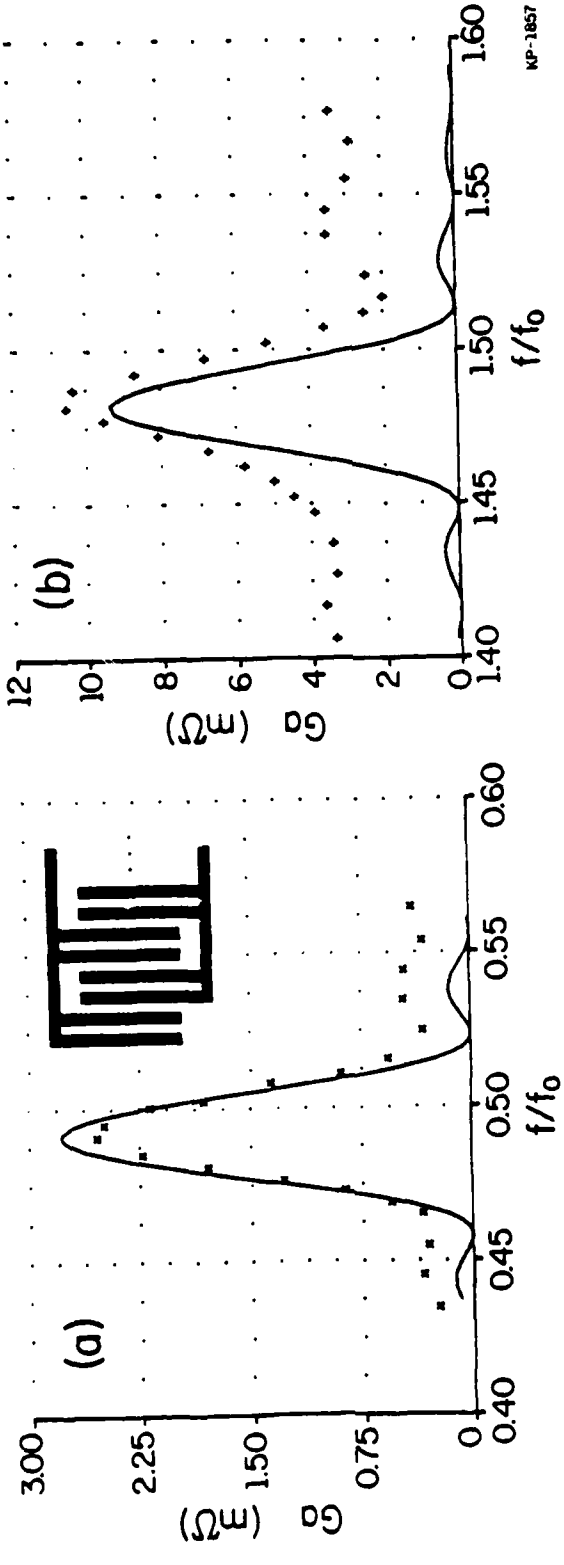

Figure 7. Radiation conductance of a 15-pair double electrode transducer. (a) Lower passband. (b) Upper passband.

$$\begin{bmatrix} m_{11} - \dfrac{m_{13}m_{31}}{m_{33\ iso}} & m_{12} - \dfrac{m_{13}m_{32}}{m_{33\ iso}} \\ m_{21} - \dfrac{m_{23}m_{31}}{m_{33\ iso}} & m_{22} - \dfrac{m_{23}m_{32}}{m_{33\ iso}} \end{bmatrix} \tag{33}$$

This two port matrix completely defines the open circuit, three port, unit cell in an isolated array.

As an example, consider the case of one electrode in an infinite array. At center frequency the single electrode acoustic reflection coefficient magnitude for the open and short circuit cases are equal (at 0.5 duty factor) and on Y-Z lithium niobate the value of 0.01647 agrees well with experimental results [16-19]. For the case of double electrodes (ie. 0.5 duty factor electrodes connected in pairs), the calculated coupling coefficient at fundamental is reduced by a factor of 0.736 from the single electrode case. This predicts a piezoelectric transducer coupling factor $K_s = (0.046X0.736)^{1/2} = 0.184$ compared to the experimental value of 0.193 [12].

To find the reflection and transmission coefficients of isolated electrode arrays, the single electrode scattering matrix (33) is cascaded as in section III.A. (the non-acoustic terms are set equal to zero). The calculated array acoustic transmission coefficients (shorted and open cases) are compared with experiment [21] (bars) for three duty factors in Fig. 8. The device is a 100 electrode array on Y-Z lithium niobate. The experimental values of single electrode normalized impedance (z in [21]) are used in the author's transmission line equation (with N = 100 and duty

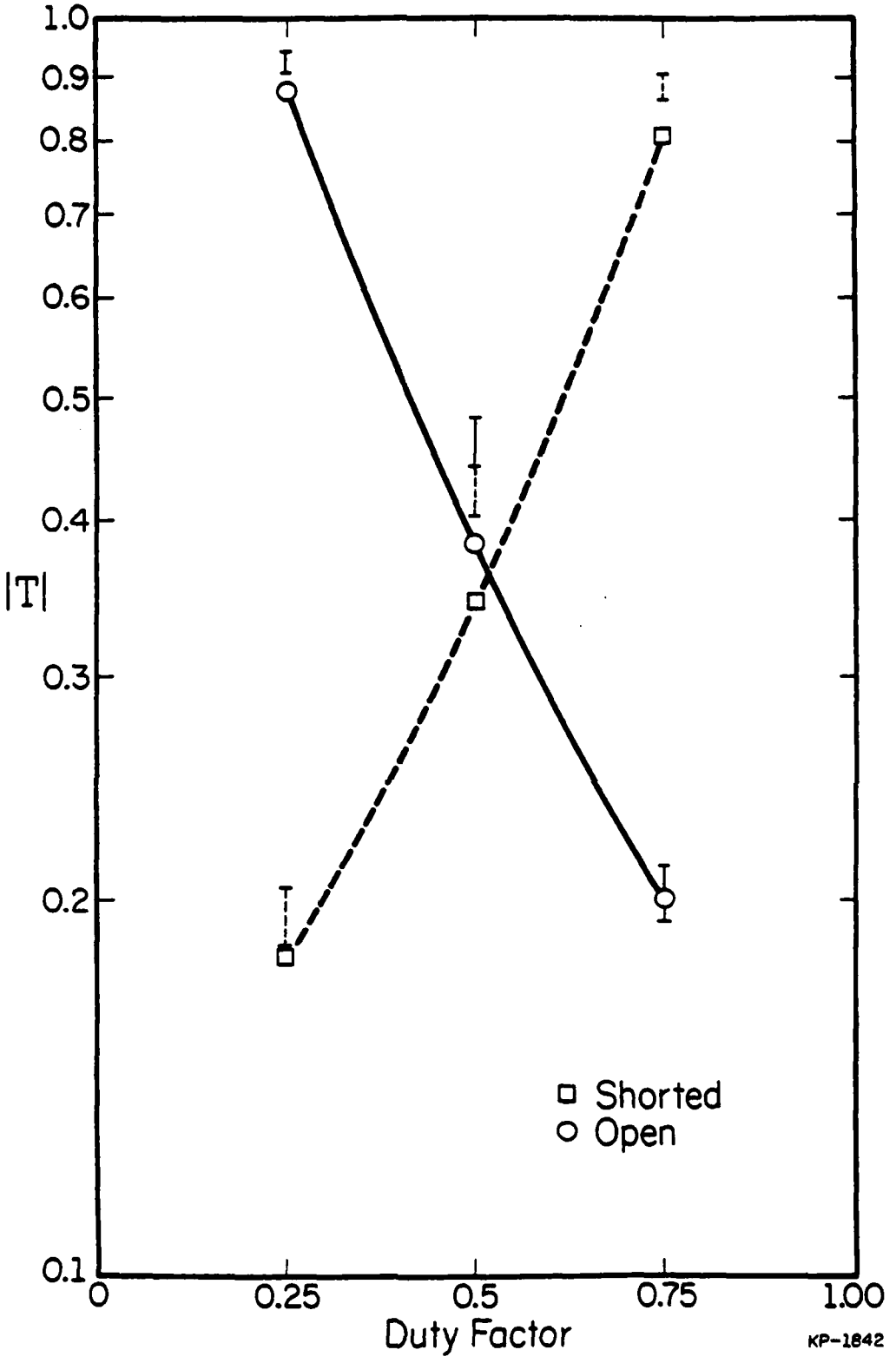

Figure 8. Transmission coefficient versus duty factor for a shorted and open (isolated) 100 electrode reflector on Y-Z lithium niobate.

factor = t_m (author's notation) = 0.5) to calculate the array reflection and transmission coefficients:

$$R = \frac{z' - 1}{z' + 1} \qquad |T| = (1 - |R|^2)^{1/2} \tag{34}$$

where $z' = z^{2N}$ for the short circuit and $z' = z^{-2N}$ for the open circuit case. Good agreement with experiment is found in Fig. 9 where the transmission coefficient ($T = 10*\log_{10}(M_{21})$) of this 100 electrode array is plotted versus frequency.

The device transmission coefficient (M_{21}) is a complex number whose phase describes the dispersion of finite length reflector and transducer arrays. The fractional acoustic transmission coefficient phase shift ($\Delta\phi_{21}/\phi_{21}$) is defined as

$$\frac{\Delta\phi_{21}}{\phi_{21}} = \frac{N\pi f/f_o - \phi_{21}}{N\pi f/f_o} \tag{35}$$

where $N\pi f/f_o$ is the open surface phase delay. This fractional phase shift is equal to the fractional shift in velocity $\Delta v/v$ and is compared with experiment (duty factor = η = 0.5) [22] in Fig. 10 for an 80 electrode device on Y-Z lithium niobate at three duty factors. This calculation is for three possible electrode connection sequences: all connected (shorted) in Fig. 10a, every other electrode connected together (open circuit IDT) in Fig. 10b, and all electrodes unconnected (isolated array) in Fig. 10c. The highly dispersive nature of the curves near the fundamental and second harmonic is evidence of a large number of reflections in the arrays. This region is denoted as a stopband. It is interesting to note that the

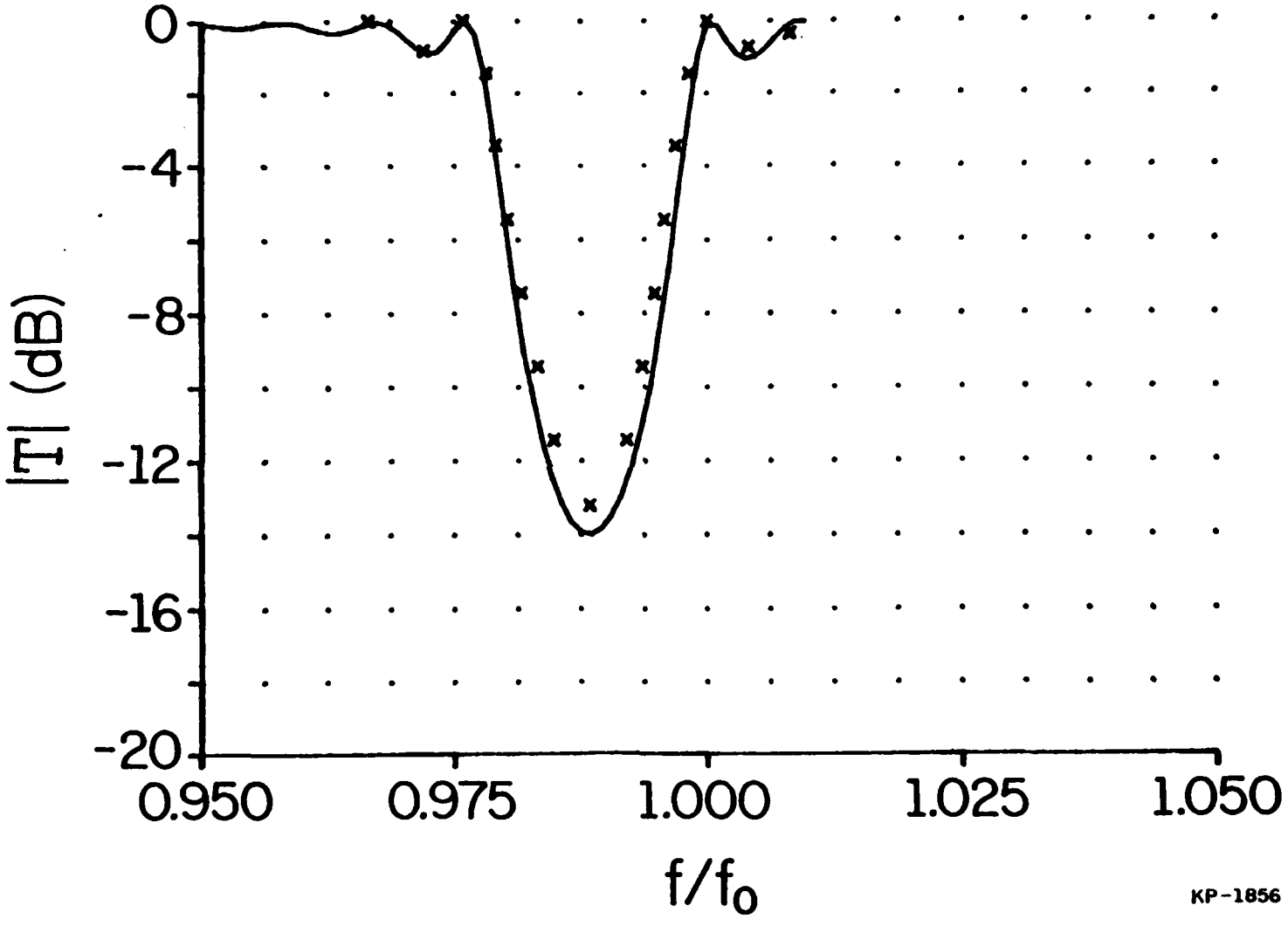

Figure 9. Open circuit transmission coefficient versus frequency (0.75 duty factor).

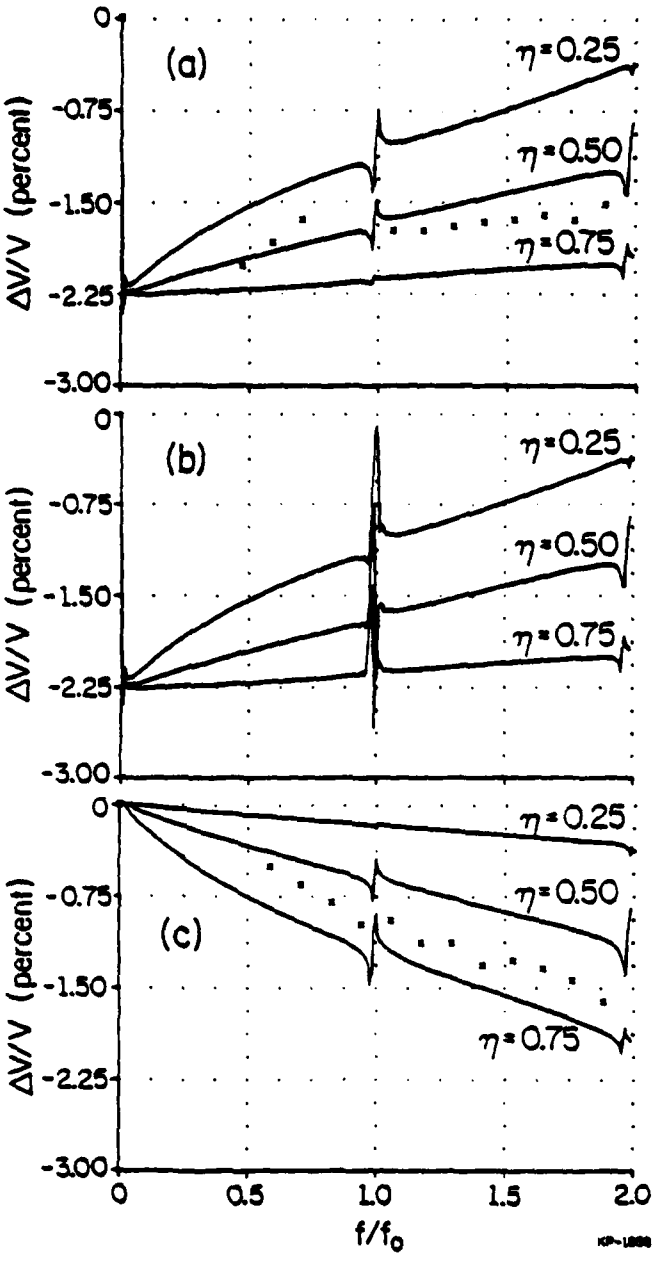

Figure 10. Normalized relative acoustic transmission phase shift versus frequency (80 electrodes) for three duty factors, experiment (x x x) at 0.5 duty factor. (a) Shorted array. (b) Open circuit transducer. (c) Isolated array.

shorted and open transducers (Fig. 10a and b, respectively) have identical dispersion characteristics out of this band. The value of $\Delta v/v$ at the fundamental stopband corresponds to the 1.7% fractional shift in frequency evident in all the devices discussed (for example, see Fig. 6). All three connection sequences display the presence of a second harmonic stopband which is also shifted downward in frequency.

D. Mechanically Loaded Transducers

A recently derived method of calculating the mechanical scattering coefficients [27,28] allows this scattering matrix cascading process to include the effects of elastic loading, mass loading, and stored energy in thick electrodes, grooves and buried electrodes. The mechanical coefficients (as in the piezoelectric case (2a,b)) are reflection coefficient and transmission phase shift for the unit cell and are composed of contributions due to linear (impedance mismatch) and quadratic (stored energy) effects

$$\begin{aligned} m_{11\ \mathrm{mech}} &= j(r_1(h/\lambda) + r_2(h/\lambda)^2) \\ j\Delta_{21\ \mathrm{mech}} &= j(\Delta_1(h/\lambda) + \Delta_2(h/\lambda)^2) \end{aligned} \tag{36}$$

and at the present are valid for frequencies about the harmonics. The derivation of these constants (r_1, r_2, Δ_1, Δ_2) is found in reference 28 (specifically equations 24 and 26) and first order examples of the calculations are found in reference 27. The mechanical coefficients (36) are added to the initial piezoelectric scattering coefficients (from (2a,b), where $j\Delta_{21\ \mathrm{piezo}} = j\Delta$ from m'_{21}) to give the composite terms

$$\begin{aligned} m'_{11\ \mathrm{total}} &= m'_{11\ \mathrm{piezo}} + m_{11\ \mathrm{mech}} \\ j\Delta_{21\ \mathrm{total}} &= j\Delta_{21\ \mathrm{piezo}} + j\Delta_{21\ \mathrm{mech}} \end{aligned} \tag{37}$$

which are used in the energy balance (5,6), thereby effecting a complete scattering analysis.

An example of the mechanical scattering contribution is shown in Fig. 11 where the calculated input radiation conductance is plotted versus frequency. This is compared with experiment [24] for a 10-pair, single electrode interdigital transducer (duty factor = 0.5). The major reflection mechanism of the transducer in Fig. 11a with 1500 Å thick aluminum electrodes is piezoelectric loading (localized shorting of the traveling potenial wave under the electrode). The effect of combined piezoelectric and mechanical loading is shown in Fig. 11b where 750 Å of gold has been added to the transducer of Fig. 11a. Although the calculated magnitudes are high, the frequency shifts of the upper zeroes are accurately predicted by this analysis. Many authors have attributed lowered experimental magnitudes to scattering into bulk waves and viscous dampening of the surface wave.

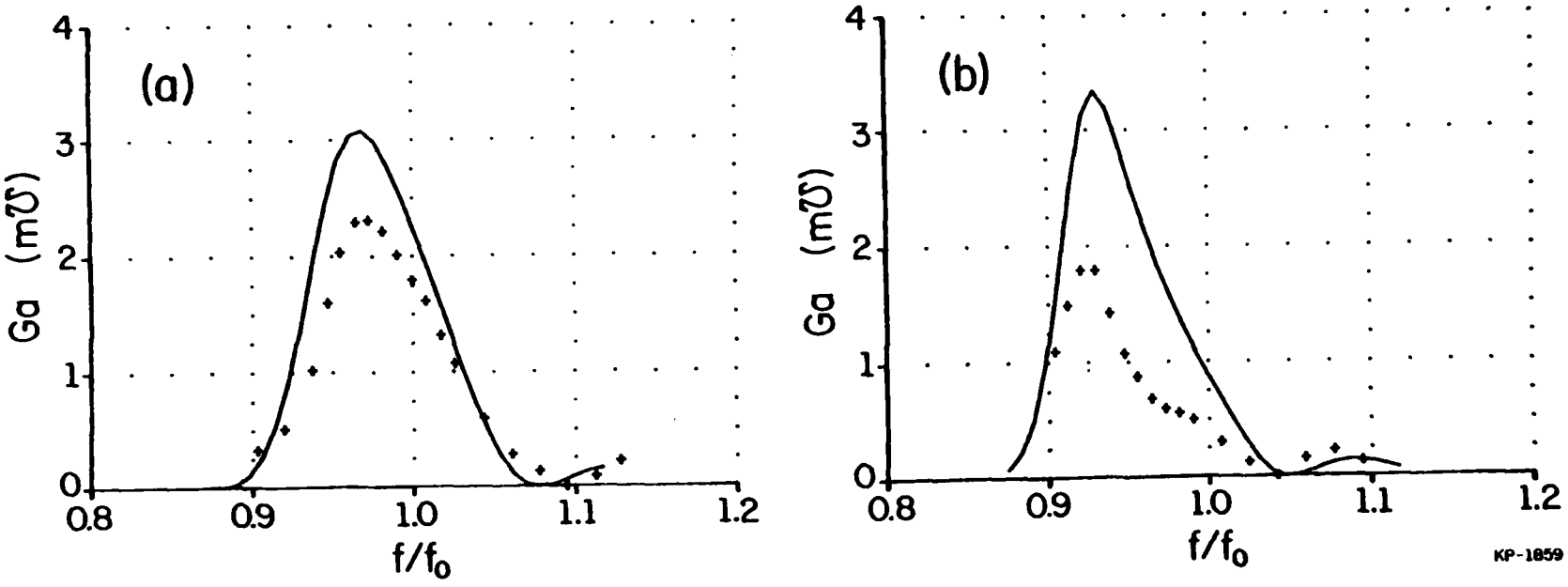

Figure 11. Radiation conductance of a 20 electrode interdigital transducer on Y-Z lithium niobate, including the effect of mass loading. (a) 1500 Å thick aluminum electrodes. (b) Same as (a) with 750 Å of gold added.

V. Transducers with Floating Electrodes

Transducers whose electrodes are individually connected to external loads and/or each other are analyzed in a straight-forward manner using this generalized scattering matrix approach. The discussion of section III. dealt with electrodes whose voltages were known apriori, whereas this section deals with transducers which contain contain floating (unconnected) electrodes in combination with connected electrodes. Reflector arrays of floating (isolated) electrodes have been treated in section IV.D. where the current through each electrically unloaded electrode was a known value (zero). This section addresses itself to a similar problem (each floating electrode current equals zero), but uses circuit analysis techniques to determine the unknown voltages. These voltages are then used to derive the 3 x 3 matrix [M] by solving for the individual scattering parameters in a manner similar to the compacting sequence of section III. Although the floating electrodes discussed are electrically isolated, this is in fact a specific case of electrodes which are externally electrically loaded. In another case, the electrodes could be connected in groups to a load (load current = $-V_T Y_L$) or to individual loads Y_{Li}, where the load currents equal $-V_i Y_{Li}$.

As an example, consider a solid electrode interdigital transducer with a floating electrode placed between each transducer electrode (the split-isolated transducer, Fig. 12 inset). The relationships between the unconnected electrode voltages (voltage tap weights) are not known, as was the case for the transducer discussed in section III., therefore the current (ie. admittance/voltage) of an electrode in this array of unknown voltages cannot be calculated directly (as was the case in (11)).

The derivation of [M] begins by cascading single electrode matrices [m] which have no capacitive electrostatic admittance (C=0). This general matrix (similar to (22))

$$\begin{bmatrix} B_1 \\ A_{N+1} \\ I_1 \\ I_2 \\ \cdot \\ \cdot \\ \cdot \\ I_N \end{bmatrix} = \begin{bmatrix} m_{11} & m_{12} & m_{13} & m_{14} & \cdot & \cdot & \cdot \\ m_{21} & m_{22} & m_{23} & m_{24} & \cdot & \cdot & \cdot \\ m_{31} & m_{32} & m_{33} & m_{34} & \cdot & \cdot & \cdot \\ m_{41} & m_{42} & m_{43} & m_{44} & \cdot & \cdot & \cdot \\ \cdot & \cdot & \cdot & \cdot & \cdot & \cdot & \cdot \\ \cdot & \cdot & \cdot & \cdot & \cdot & \cdot & \cdot \\ \cdot & \cdot & \cdot & \cdot & \cdot & \cdot & \cdot \\ \cdot & \cdot & \cdot & \cdot & \cdot & \cdot & \cdot \end{bmatrix} \begin{bmatrix} A_1 \\ B_{N+1} \\ V_1 \\ V_2 \\ \cdot \\ \cdot \\ \cdot \\ V_N \end{bmatrix} \tag{38}$$

models all the relationships (except capacitive coupling) between the electrodes. The admittance terms enclosed by the dashed line are the cascaded complex admittances ($G_a + jB_a$). Added to this sub-matrix is an inter-electrode capacitive admittance (calculated from equations (8), (9) in [2]) which models the capacitive coupling between the electrodes.

The first step in the solution of the floating electrode voltages is to combine the rows and columns associated with the transducer (connected) electrodes. This is done using the same technique as in section III.B. The matrix is now a function of two types of acoustically induced potentials, a terminal (transducer) voltage (V_T) and a set of floating electrode voltages (V_{F1} through V_{Ff}).

$$\begin{bmatrix} B_1 \\ A_{N+1} \\ I_T \\ 0 \\ \cdot \\ \cdot \\ \cdot \\ 0 \end{bmatrix} = \begin{bmatrix} m_{11} & m_{12} & m_{13} & m_{14} & \cdots \\ m_{21} & m_{22} & m_{23} & m_{24} & \cdots \\ m_{31} & m_{32} & m_{33} & m_{34} & \cdots \\ m_{41} & m_{42} & m_{43} & m_{44} & \cdots \\ \cdot & \cdot & \cdot & \cdot & \cdots \\ \cdot & \cdot & \cdot & \cdot & \cdots \\ \cdot & \cdot & \cdot & \cdot & \cdots \\ \cdot & \cdot & \cdot & \cdot & \cdots \end{bmatrix} \begin{bmatrix} A_1 \\ B_{N+1} \\ V_T \\ V_{F1} \\ \cdot \\ \cdot \\ \cdot \\ V_{Ff} \end{bmatrix} \tag{39}$$

Note, there may be more than one terminal voltage if the transducer has multiple groups of taps connected together (ie. group-type unidirectional).

An examination of (39) shows that the induced currents (and hence, the floating electrode voltages) are functions of each other, the terminal voltage and the incident acoustic waves. There are three different sets of floating voltages corresponding to the three possible excitation sources (V_T, A_1, B_{N+1}), each taken one at a time. For example, the value of M_{13} is defined as the traveling acoustic wave emerging from the left port due to the terminal voltage applied with the incident waves absent.

The second step is to use one of the excitation sources as the appropriate bondary condition and solve the admittance sub-matrix for the three sets of floating voltages. This is done by multiplying the first three columns (39) by the appropriate boundary conditions (each 0 or 1). The Gauss-Seidel iteration method [25] is used three separate times to solve this new f by f+3 sub-matrix for the unknown floating electrode voltages. The inversion of the admittance matrix is not required and

consequently very large matrices may be analyzed.

The third step is to solve for the device matrix [M] by using the floating electrode voltages in (40) to combine the columns and rows as in section III. (for an unconnected electrode b_i is 0). This is done for each of the three excitation sources.

As an example, consider the solution of the first column in the device matrix (M_{11}, M_{21}, M_{31}). These scattering parameters are defined as the two acoustic waves and terminal current produced by an incident acoustic wave from the left when the device is shorted (in this split-isolated case, a shorted transducer) and the incident wave from the right is not present. Let B_{N+1} and V_T equal zero and the incident wave (A_1) equal one.

$$\begin{bmatrix} B_1 \\ A_{N+1} \\ I_T \\ 0 \\ . \\ . \\ . \\ 0 \end{bmatrix} = \begin{bmatrix} m_{11} & m_{12} & m_{13} & m_{14} & \cdots \\ m_{21} & m_{22} & m_{23} & m_{24} & \cdots \\ m_{31} & m_{32} & m_{33} & m_{34} & \cdots \\ m_{41} & m_{42} & m_{43} & m_{44} & \cdots \\ . & . & . & . & \cdots \\ . & . & . & . & \cdots \\ . & . & . & . & \cdots \\ . & . & . & . & \cdots \end{bmatrix} \begin{bmatrix} 1 \\ 0 \\ 0 \\ V_{F1} \\ . \\ . \\ . \\ V_{Ff} \end{bmatrix} \qquad (40)$$

After multiplication of the first three columns (accounting for the boundary conditions) the sub matrix is

$$\begin{bmatrix} m_{41} & 0 & 0 & m_{44} & m_{45} & m_{46} \cdots m_{4,f+3} \\ m_{51} & 0 & 0 & m_{54} & m_{55} & m_{56} \cdots m_{5,f+3} \\ m_{61} & 0 & 0 & m_{64} & m_{65} & m_{66} \cdots m_{6,f+3} \\ \cdot & \cdot & \cdot & \cdot & \cdot & \cdot \cdots \cdot \\ \cdot & \cdot & \cdot & \cdot & \cdot & \cdot \cdots \cdot \\ \cdot & \cdot & \cdot & \cdot & \cdot & \cdot \cdots \cdot \\ m_{f1} & 0 & 0 & m_{f4} & m_{f5} & m_{f6} \cdots m_{f,f+3} \end{bmatrix} \tag{41}$$

After solving the floating voltages from these f equations, the desired coefficients are the first three rows (m=1, 2, 3) multiplied by the external boundary conditions and the potentials:

$$\begin{aligned} M_{11} &= m_{11}*1 + m_{12}*0 + m_{13}*0 + m_{14}*V_{F1} + \cdots + m_{1f}*V_{Ff} \\ M_{21} &= m_{21}*1 + m_{22}*0 + m_{23}*0 + m_{24}*V_{F1} + \cdots + m_{2f}*V_{Ff} \\ M_{31} &= m_{31}*1 + m_{32}*0 + m_{33}*0 + m_{34}*V_{F1} + \cdots + m_{3f}*V_{Ff} \end{aligned} \tag{42}$$

Similar steps are taken to derive the other six device matrix [M] parameters. This matrix

$$\begin{bmatrix} B_1 \\ A_{N+1} \\ I_T \end{bmatrix} = \begin{bmatrix} M_{11} & M_{12} & M_{13} \\ M_{21} & M_{22} & M_{23} \\ M_{31} & M_{32} & M_{33} \end{bmatrix} \begin{bmatrix} A_1 \\ B_{N+1} \\ V_T \end{bmatrix} \tag{43}$$

completely defines the transducer with floating electrodes and is used to derive the electrically loaded parameters via (29-31).

A comparison of the calculated acoustic reflection coefficient with that measured for a 20 wavelength split-isolated transducer (duty factor = 0.5) on Y-Z lithium niobate (Fig. 12) [14] shows good agreement with experiment for the cases of short ($r_{sc} = M_{11}$) and open circuit ($r_{oc} = M_{11} + M_{13}M_{31}/M_{33}$, from (31)) transducers. The difference between experimental and calculated magnitudes can be attributed to viscous damping and surface wave scattering into bulk waves which are not reflected. Nonetheless, the analysis has predicted the reflection coefficient shape and null frequencies quite well.

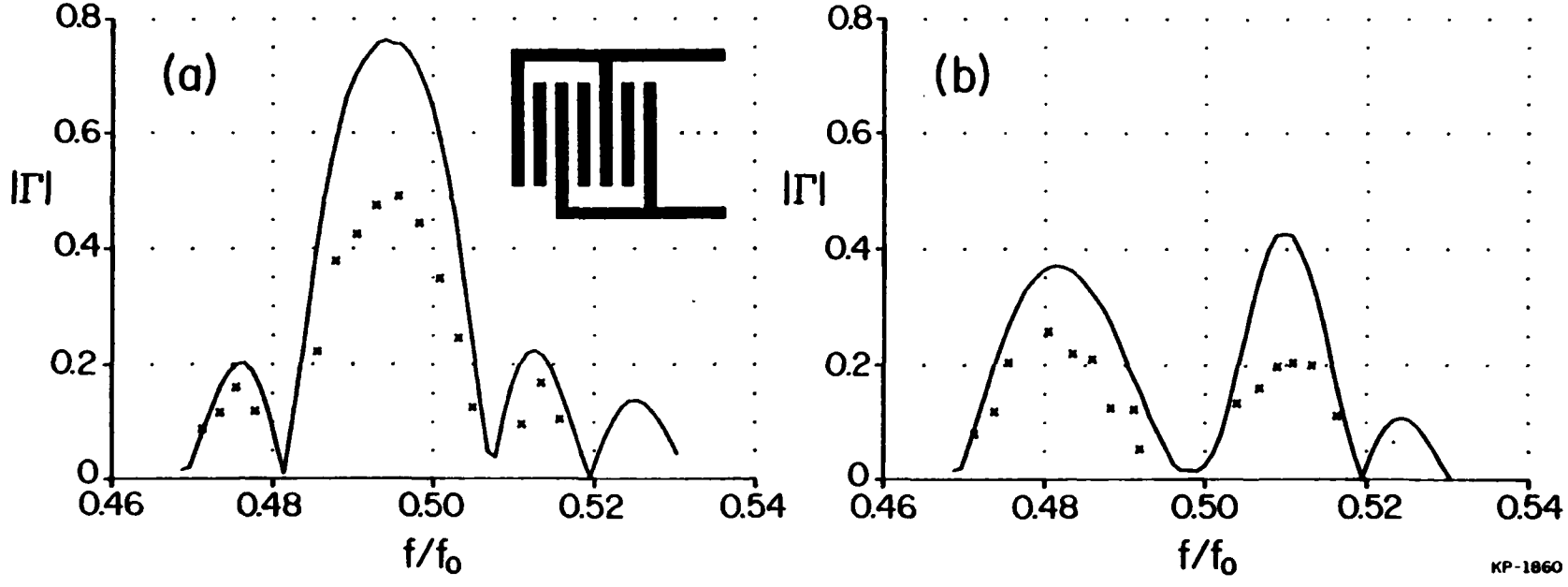

Figure 12. Reflection coefficient magnitude for split-isolated transducer. (a) Transducer short circuited. (b) Transducer open circuited.

VI. Conclusion

This work has modified and corrected the phased periodic array scattering parameters for use as a single electrode (unit cell) scattering matrix. The analytical expressions upon which this matrix is based are functions of material constants, electrode geometry and frequency. These single electrode, three port scattering matrices are acoustically cascaded to produce an array scattering matrix which completely describes the device, be it reflector, transducer or combination. The analysis takes into account the effects of both piezoelectric and mechanical scattering and provides all device transfer functions versus frequency. By virtue of the scattering matrix approach, the final 3-port matrix includes all finger interactions such as acoustic reflections and electrical regeneration regardless of individual electrode circuitry. The calculation is a straight-forward procedure and is applicable to any uniform beam-width, periodic electrode configuration (including the case of transducers with floating electrodes). Good agreement with experimental data confirms this approach to be a universal and accurate analysis tool.

Appendix I.

A. Derivation of radiation conductance (G_a)

The conservation of energy for a lossless symmetrical interdigital electrode requires the electrical input power to equal the total acoustic output power. That is, with a voltage V applied

$$G_a \frac{V^2}{2} = \mathrm{Re}(m_{33}) \frac{V^2}{2} = \frac{|V\, m_{13}|^2}{2\, Z_0} + \frac{|V\, m_{23}|^2}{2\, Z_0} \qquad \text{(A1)}$$

dividing both sides by $\frac{V^2}{2}$ gives

$$G_a = \frac{m_{13}\, m^*_{13}}{Z_0} + \frac{m_{23}\, m^*_{23}}{Z_0} \qquad \text{(A2)}$$

replacing m^*_{13} and m^*_{23} with

$$m_{13} = \frac{-Z_0\, m_{31}}{2} \qquad m_{23} = \frac{-Z_0\, m_{32}}{2} \qquad \text{(A3)}$$

from appendix I. B. gives equation (7)

$$G_a = -.5(m_{13} m^*_{31} + m_{23} m^*_{32}). \qquad \text{(A4)}$$

B. Derivation of the relationship between m_{13} and m_{31}

The relationship between mixed units and pure units scattering matrices has been discussed for the two port case by Viggh [26]. This appendix extends his work to the three port case in order to derive the relationship between the mixed units m_{13} and m_{31}. For clarity of presentation, the mixed units and pure acoustic scattering matrices will be designated by [m] and [s], respectively.

The variables of the mixed units electrical port are voltage and current. Their relationship to an acoustic representation is via

$$\begin{aligned} v_3 &= a_3 + b_3 \\ Z_0\, i_3 &= a_3 - b_3 \end{aligned} \tag{A5}$$

where Z_0 is the electro-acoustic charactersitic impedance (8). The problem is to write the three port acoustic scattering matrix (where a_i and b_i are the input and output acoustic wave potentials, respectively)

$$\begin{bmatrix} b_1 \\ b_2 \\ b_3 \end{bmatrix} = \begin{bmatrix} s_{11} & s_{12} & s_{13} \\ s_{21} & s_{22} & s_{23} \\ s_{31} & s_{32} & s_{33} \end{bmatrix} \begin{bmatrix} a_1 \\ a_2 \\ a_3 \end{bmatrix} \tag{A6}$$

in terms of the mixed units matrix (similar to (1))

$$\begin{bmatrix} b_1 \\ b_2 \\ i_3 \end{bmatrix} = \begin{bmatrix} m_{11} & m_{12} & m_{13} \\ m_{21} & m_{22} & m_{23} \\ m_{31} & m_{32} & m_{33} \end{bmatrix} \begin{bmatrix} a_1 \\ a_2 \\ v_3 \end{bmatrix} \tag{A7}$$

Starting with the third mixed units equation, insert (A5) for the current and voltage

$$\frac{a_3 - b_3}{Z_0} = m_{31}a_1 + m_{32}a_2 + m_{33}(a_3 + b_3) \tag{A8}$$

Rearranging terms and solving for b_3 produces the third acoustic scattering equation

$$b_3 = \frac{-Z_0 m_{31}}{1+Z_0 m_{33}} a_1 + \frac{-Z_0 m_{32}}{1+Z_0 m_{33}} a_2 + \frac{1-Z_0 m_{33}}{1+Z_0 m_{33}} a_3 \tag{A9}$$

The next step uses the first mixed equation to produce the first acoustic equation

$$\begin{aligned} b_1 &= m_{11}a_1 + m_{12}a_2 + m_{13}v_3 \\ &= m_{11}a_1 + m_{12}a_2 + m_{13}(a_3 + b_3). \end{aligned} \tag{A10}$$

From (A6) we know

$$b_3 = s_{31}a_1 + s_{32}a_2 + s_{33}a_3. \tag{A11}$$

and therefore,

$$b_1 = (m_{11} + m_{13}s_{31})a_1 + (m_{12} + m_{13}s_{32})a_2 + m_{13}(1 + s_{33})a_3 \tag{A12}$$

A similar equation exists for b_2.

In summary, the acoustic scattering matrix [s] (A6) in terms of the mixed units representation is

$$\begin{bmatrix} b_1 \\ b_2 \\ b_3 \end{bmatrix} = \begin{bmatrix} (m_{11} + m_{13}s_{31}) & (m_{12} + m_{13}s_{32}) & m_{13}(1+s_{33}) \\ (m_{21} + m_{23}s_{31}) & (m_{22} + m_{23}s_{32}) & m_{23}(1+s_{33}) \\ \dfrac{-Z_0 m_{31}}{1+Z_0 m_{33}} & \dfrac{-Z_0 m_{32}}{1+Z_0 m_{33}} & \dfrac{1-Z_0 m_{33}}{1+Z_0 m_{33}} \end{bmatrix} \begin{bmatrix} a_1 \\ a_2 \\ a_3 \end{bmatrix} \tag{A13}$$

A symmetrical, lossless, reciprocal 3-port has the property that $s_{13} = s_{31}$. Therefore, using the transformation (A13) we find

$$m_{13}(1 + s_{33}) = \frac{-Z_0 m_{31}}{1+Z_0 m_{33}} \tag{A14a}$$

and

$$m_{13}\frac{2}{1+Z_0 m_{33}} = \frac{-Z_0 m_{31}}{1+Z_0 m_{33}} \tag{A14b}$$

producing the desired result

$$m_{13} = \frac{-Z_0\ m_{31}}{2}. \tag{A15}$$

Appendix II. Scattering Matrix Cascading

The problem addressed in this appendix is to find the resultant acoustic potentials B_1, A_3 and the currents produced for the case where the incident acoustic potentials A_1, B_3 and the voltages applied are known. In this case the imaginary admittance is known and the largest matrix is N+2 by 3.

The first scattering matrix (which could be the entire matrix [M] to the left of this point) is written in equation form as

$$\begin{aligned} B_1 &= M_{11}A_1 + M_{12}B_2 + M_{13}V_T \\ A_2 &= M_{21}A_1 + M_{22}B_2 + M_{23}V_T \\ I_1 &= M_{31}A_1 + M_{32}B_2 + M_{33}V_T \end{aligned} \tag{A16}$$

where the M_{13} have been multiplied by the tap weight (ie. the voltage applied as a fraction of the terminal voltage). The set of equations characterizing the tap to be appended is

$$\begin{aligned} B_2 &= m_{11}A_2 + m_{12}B_3 + m_{13}V_T \\ A_3 &= m_{21}A_2 + m_{22}B_3 + m_{23}V_T \\ I_2 &= m_{31}A_2 + m_{32}B_3 + m_{33}V_T \end{aligned} \tag{A17}$$

Comparing the matrix equations shows that there are two equations that contain A_2 in terms of B_2 and the known quantities (incident acoustic waves and voltage tap weights). These are solved as follows, taking the second set first

$$B_2 = m_{11}A_2 + m_{12}B_3 + m_{13}V_T \tag{A18a}$$

inserting an equation for A_2 gives

$$B_2 = m_{11}(M_{21}A_1 + M_{22}B_2 + M_{23}) + m_{12}B_3 + m_{13}V_T \tag{A18b}$$

and

$$B_2 = \frac{m_{11}(M_{21}A_1 + M_{23})}{1 - m_{11}M_{22}} + m_{12}B_3 + m_{13}V_T \quad \text{(A18c)}$$

which is written as

$$B_2 = C_1A_1 + C_2B_3 + C_3V_T \quad \text{(A19)}$$

where

$$C_1 = \frac{m_{11}M_{21}}{1 - m_{11}M_{22}} \quad \text{(A20a)}$$

$$C_2 = \frac{m_{12}}{1 - m_{11}M_{22}} \quad \text{(A20b)}$$

$$C_3 = \frac{m_{11}M_{23} + m_{13}V_T}{1 - m_{11}M_{22}} \quad \text{(A20c)}$$

Similarly

$$A_2 = M_{21}A_1 + M_{22}B_2 + M_{23}V_T \quad \text{(A21a)}$$

is written as

$$A_2 = D_1A_1 + D_2B_3 + D_3V_T \quad \text{(A21b)}$$

where

$$D_1 = M_{21} + M_{22}C_1 \quad \text{(A22a)}$$

$$D_2 = M_{22}C_2 \quad \text{(A22b)}$$

$$D_3 = M_{22}C_3 + M_{23} \quad \text{(A22c)}$$

These solutions are inserted into the proper equations in the two matrices (A16, A17) and a new 3 by 4 array matrix is created in terms of the new input parameters

$$\begin{aligned} B_1 &= M_{11}A_1 + M_{12}(C_1A_1 + C_2B_3 + C_3) + M_{13}V_T \\ A_3 &= m_{21}(D_1A_1 + B_3D_2 + D_3) + m_{22}B_3 + m_{23}V_T \\ I_1 &= M_{31}A_1 + M_{32}(C_1A_1 + C_2B_3 + C_3) + M_{33}V_T \\ I_2 &= m_{31}(D_1A_1 + D_2B_3 + D_3) + m_{32}B_3 + m_{33}V_T \end{aligned} \quad \text{(A23)}$$

Therefore a new M matrix of the form

$$\begin{bmatrix} M_{11} + C_1M_{12} & C_2M_{12} & C_3M_{12} + M_{13} \\ D_1m_{21} & D_2m_{21} + m_{22} & D_3m_{21} + m_{23} \\ M_{31} + C_1M_{32} & C_2M_{32} & C_3M_{32} + M_{33} \\ D_1m_{31} & D_2m_{31} + m_{32} & D_3m_{31} + m_{33} \end{bmatrix} \tag{A24}$$

has been created from the original two scattering matrices. This matrix relates the input acoustic potentials (A_1,B_3) and the terminal voltage applied (V_T) to the output acoustic potentials (A_3, B_1) and the currents produced. The procedure can be carried out for N taps with a resulting N+2 by 3 scatter matrix for the entire array.

References:

1. S. Datta and B. J. Hunsinger, "An analytical theory for piezoelectric scattering by periodic arrays," submitted to J. of App. Phys.

2. S. Datta and B. J. Hunsinger, "Element factor for periodic transducers," IEEE. Trans. Sonics Ultrason., vol. SU-27, January 1980.

3. R. M. White, "Surface elastic-wave propagation and amplification," IEEE Trans. Electron. Devices, vol. ED-14, pp.181-189, April 1967.

4. W. R. Smith, H. M. Gerard, J. H. Collins, T. M. Reeder, and H. J. Shaw, "Analysis of interdigital surface wave transducers by use of an equivalent circuit model," IEEE Trans. Microwave Theory Tech., vol. MTT-17, pp. 856-864, November 1975.

5. W. P. Mason, Electromechanical Transducers and Wave Filters, 2nd edition, Princeton, N.J.: VanNostrand, 1948, pp. 201-209, 399-409.

6. C. S. Hartmann, D. T. Bell, and R. C. Rosenfeld, "Impulse model design of acoustic surface-wave filters," IEEE Trans. Microwave Theory Tech., vol. MTT-21, pp.162-175, April 1973.

7. H. Engan, "Excitation of elastic surface waves by spatial harmonics of interdigital transducers," IEEE Trans. Electron. Devices, vol. ED-16, pp. 1014-1017, December 1969.

8. R. H. Tacrell and M. G. Holland, "Acoustic surface wave filters," Proc. IEEE, vol. 59, pp. 393-409, March 1971.

9. W. R. Smith and W. F. Pedler, "Fundamental- and harmonic-frequency circuit-model analysis of interdigital transducers with arbitrary metallization ratios and polarity sequences," IEEE Trans. Microwave Theory Tech., vol. MTT-23, pp. 853-864,

November 1975.

10. T. L. Szabo, K. R. Laker, and E. Cohen, "Interdigital transducer models: their impact on filter synthesis," IEEE Trans. Sonics Ultrason., vol. SU-26, pp. 321-333, September 1979.

11. S. Datta, B. J. Hunsinger, and D. C. Malocha, "A generalized model for periodic transducers with arbitrary voltages," IEEE Trans. Sonics Ultrason., vol. SU-26, pp. 235-242, May 1979.

12. T. Aoki and K. A. Ingebrigtsen, "Equivalent circuit parameters of interdigital transducers derived from dispersion relations for surface acoustic waves in periodic metal gratings," IEEE Trans. Sonics Ultrason., vol. SU-24, pp. 167-178, May 1977.

13. T. Aoki and S. Hattori, "Equivalent circuit parameters for harmonic operation of SAW transducer," 1977 IEEE Ultrasonics Symp. Proc., pp.653-658.

14. A. J. DeVries, R. L. Miller and T. J. Wojcik, "Reflection of a surface wave from three types of ID transducers," 1972 IEEE Ultrasonic Symp. Proc., pp.353-358.

15. A. J. DeVries and S. Subramanian, "Overall comparison between theoretical predictions using the cross-field transmission-line model and experimental measurements of a split-connected transducer, 1973 IEEE Ultrasonic Symp. Proc., pp.407-409.

16. W. S. Jones, C. S. Hartmann and T. D. Strudivant, "Second order effects in surface wave devices," IEEE Trans. Sonics Ultrason., vol. SU-19, pp. 368-377, July 1972.

17. W. R. Smith, "Experimental distinction between cross-field and in-line three port circuit models for interdigital transducers," IEEE Trans. Microwave Theory Tech., vol. MTT-22, pp.960-964,

November 1974.

18. E. J. Staples, et al., "UHF surface acoustic wave resonators," 1974 IEEE Ultrasonics Symp. Proc., pp. 245-252.

19. K. M. Lakin, et al., "Planar surface acoustic wave resonators," ibid., pp.263-267.

20. H. Engan, "Surface acoustic wave multielectrode transducers, IEEE Trans. Sonics Ultrason., vol. SU-22, pp. 395-401, November 1975.

21. G. L. Matthaei, "S.A.W. reflecting arrays", Electronics Letters, Vol. 12, No. 21, October 14, 1976.

22. R. C. Williamson, "Measurement of the propagation characteristics of surface and bulk waves in $LiNbO_3$," 1972 IEEE Ultrasonics Symp. Proc., pp. 323-327.

23. D. M. Kerns and R. W. Beatty, Basic Theory of Waveguide Junctions and Introductory Microwave Network Analysis, 1st edition, 1967: Pergamon Press, pp. 97-109.

24. H. Skeie, "Electrical and mechanical loading of a piezoelectric surface supporting surface waves," Journal of the Acoustical Society of America, vol. 48, no. 5, pp. 1098-1108, 1970.

25. C. F. Gerald, Applied Numerical Analysis, 1st edition, 1973: Addison-Wesley Publishing, pp. 154-156.

26. M. E. Viggh, "Mixed two-port parameters for characterizing varactor mounts in waveguides," IEEE Trans. Microwave Theory Tech., vol. MTT-11, pp. 218-19, May 1963.

27. S. Datta and B. J. Hunsinger, "First-order reflection reflection coefficient of surface acoustic waves from thin-strip overlays," J. of App. Phys., 50(9), September 1979.

28. S. Datta and B. J. Hunsinger, "An analysis of energy storage effects

on SAW propagation in periodic arrays," submitted to IEEE Trans. Sonics Ultrason.

29. C. C. Tseng, "Frequency response of an interdigital transducer for excitation of surface elastic waves," IEEE Trans. Electron. Devices, vol. ED-15, pp. 586-594, August 1968.

30. A. L. Nalamwar and M. Epstein, "Immittance characterization of acoustic surface wave transducers," Proc. IEEE (Lett.), vol. 60, pp.366-377, March 1972.

Vita

Carl Michael Panasik was born in Cleveland, Ohio on August 21, 1952. He received his B.E.E. at the Cleveland State University in June 1974 and his M.S. degree from the University of Illinois at Urbana-Champaign in May 1976.

His publications are

1. C. M. Panasik and B. J. Hunsinger, "Precise impulse response measurement of saw filters," IEEE Trans. Sonics Ultrason., vol. SU-23, no. 4, July 1976.
2. C. M. Panasik, "Time domain analysis of saw filters," Masters Thesis, University of Illinois at Urbana-Champaign, June 1977.
3. C. M. Panasik and B. J. Hunsinger, "Harmonic analysis of saw transducers," IEEE Trans. Microwave Theory Tech., vol. MTT-26, no.6, June 1978.

He was a Research Assistant in the Surface Acoustic Wave research group at the Coordinated Science Laboratory, University of Illinois at Urbana-Champaign until February 1980. He is currently a member of the technical staff in the Advanced Technology Laboratory at Texas Instruments Inc., Dallas, Texas.


DATE
FILME
7 - 8